UMEÅ UNIVERSITY

Trailer Simulation Model for an Indirect Tire Pressure Monitoring System

Leon Amkoff

Master thesis, 30 hp

Master's Programme in Robotics and Control, 120 hp

Spring term 2021

Abstract

A car with underinflated tires can lead to both safety and environmental issues. To combat this, markets have begun requiring new cars to feature a Tire Pressure Monitoring System. Systems without pressure sensors are referred to as indirect Tire Pressure Monitoring Systems, often utilizing wheel speed sensors in combination with other available sensor information to detect tire pressure losses.

NIRA Dynamics is a company founded in Linköping, Sweden, most known for its indirect Tire Pressure Monitoring System called TPI. TPI needs to be verified in a large number of scenarios, which may be both difficult and expensive to realize in real vehicle tests. The purpose of this master thesis was to investigate and model what physical phenomena are associated with having a trailer connected to a car, relevant for TPI. The goal was to construct a hybrid simulation framework, making it possible to modify car-only data to reflect the effects of having a trailer connected.

A car-trailer model was developed, showing close resemblance in simulations to real collected car-trailer sensor data. The model was then used to design a hybrid simulation framework, where car-only sensor signals were modified to mimic having different types of trailers attached. The hybrid simulation results show close resemblance to real collected trailer sensor data. By not requiring real trailer data for every scenario to evaluate software performance on, the proposed framework opens up the possibility to simulate data from a much larger number of trailer combinations than would otherwise have been feasible to test in real vehicle tests.

Acknowledgements

First of all I want to thank my supervisor at NIRA Dynamics - Kristoffer Lundahl - for all his guidance and time spent helping me figure things out during this project. This master thesis would not have been possible without him and for that I am truly grateful.

I want to give special thanks to Mats Widmark and Thomas Gustafsson at NIRA who also contributed with their broad vehicle dynamics knowledge, as well as always making our meetings fun and lighthearted. A big thanks to David Jonsson at the test department for great ideas regarding the test planning and data gathering, not to mention helping performing some of the actual tests. Thank you Robert Johansson for including me in all the nice team activities from day one.

Moving across Sweden from Umeå to Linköping in the middle of a pandemic was strange, but everyone at NIRA still managed to give me such a warm welcome and making my time here really enjoyable. Thank you for that!

Finally, I want to thank my supervisor at Umeå University Sven Rönnbäck and master thesis course responsible Leonid Freidovich for all their help and support, both during this thesis and throughout the master's programme.

Leon Amkoff

Linköping, June 2021

Contents

Chapter 1

Introduction

In this chapter the background to the project is described in terms of background, related work, ethics considered, purpose and goal. The theory used for parameter identification and model analysis is then described in Chapter 2. Vehicle dynamics and models describing the car-trailer system in different ways are treated in Chapter 3. The general method with preliminary results of data gathering and associated signal processing is presented in Chapter 4. The proposed hybrid simulation framework is described in Chapter 5. The main results are shown in Chapter 6. Then, the results are discussed and some improvements are suggested in Chapter 7. Finally, the project is summarized and conclusions are drawn related to limitations and future work in Chapter 8.

1.1 Background

A car with underinflated tires can lead to both safety and environmental issues. It reduces the driver vehicle handling capability, and can in extreme cases lead to a flat tire. Additionally, the more a tire is underinflated, both fuel consumption and the wear on the tire increases. In order to reduce CO_2 emissions and increase safety in cars, markets have begun requiring new cars to feature a Tire Pressure Monitoring System (TPMS). USA was first out in 2007 [1], followed by EU in 2012 [2] and later other countries such as Russia, China and Korea implemented similar legislation. These systems monitor tire pressure and warn the driver if the pressure in any tire deviates from safe levels. The estimations can either be performed direct (dTPMS) by specifically installing pressure sensor in each wheel, or indirect (iTPMS) by combining measurements from other already existing sensor signals in the car.

NIRA Dynamics AB is a company founded and based in Linköping, with close connection to Linköping University. NIRA provides software solutions for the automotive industry in vehicle onboard analytics and road perception. With installations in more than 40 Million vehicles, they are perhaps most known for their iTPMS software called TPI (Tire Pressure Indicator). TPI utilizes already existing wheel speed sensors and combines these signals with other available sensor information to detect tire pressure losses in passenger vehicles. The software can detect pressure losses in either one, two, three or all four tires simultaneously, as well as alerting the driver about which tire is underinflated. TPI is normally integrated in the car ESC (Electronic Stability Control), meaning that it can be implemented in cars without requiring any additional hardware than what is allready installed.

The algorithm process of TPI can be considered as consisting of two different detection principles. One principle monitors relative wheel speeds, and the other principle monitors wheel vibrations. An underinflated tire will have a slightly reduced radius than it otherwise would, causing the wheel to spin faster. This effect can be observed in the wheel speed signals, making it possible to detect and isolate which tire is affected. An illustration of the principle can be seen in Figure 1.1a. Apart from the wheel rolling faster, its resonance frequency also shifts and increases in amplitude, see Figure 1.1b. By using sensor fusion and signal processing algorithms, these two principles can be combined into a single robust detection system.

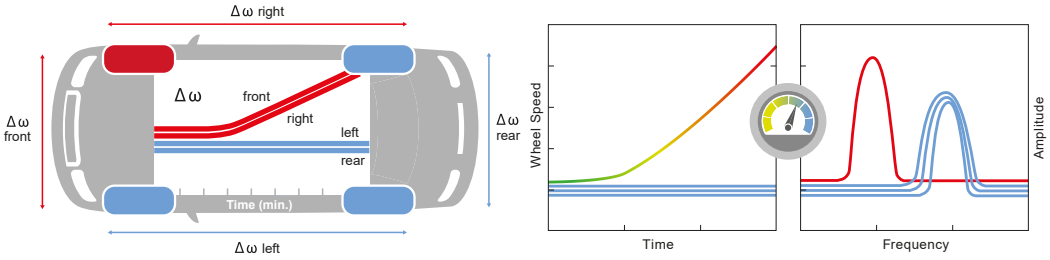

(a) Wheel speed analysis.

(b) Wheel spectrum analysis.

Figure 1.1 – TPI detects underinflation by monitoring relative wheel speeds and wheel vibration frequencies [3]. The figures illustrate the detection procedure in the case of a single tire pressure drop.

While the core of TPI is robust and has been proven to achieve full performance in many different vehicle types, it still has parameters that needs to be mapped when integrating the software in new car models. The mapping process includes extensive data collection, for example driving with different tires, tire pressures, road conditions and loads. Some of the scenarios may be both difficult and expensive to realize in real vehicle tests, making simulations a seemingly more attractive option.

However, pure simulations of the vehicle system under these different conditions would require a highly complex model, needing many parameters of its own to be estimated from real vehicle tests. An alternative approach could be taking collected in-vehicle data from some base driving scenario, and then modifying the sensor signals to reflect a slightly different scenario. The result is a hybrid simulation method, combining real sensor data with simulation models.

One of the scenarios that could benefit from being hybrid simulated at NIRA is the case when a trailer is attached to the car. The hybrid simulation method would allow evaluating TPI functionality in the scenario of having a trailer connected, using real test data logs without any trailer actually connected. Reusing car data logs this way would make the TPI verification process more time- and cost efficient. It would also open up the possibility to evaluate performance with as many types and variants of trailers as one would desire with little to no extra effort spent.

1.2 Purpose

The purpose of this master thesis is to investigate and model what physical phenomena are associated with having a trailer connected to a car, relevant for NIRA's indirect Tire Pressure Monitoring System (iTPMS) software product TPI.

1.3 Goal

The goal of this master thesis is to construct a hybrid simulation framework, making it possible to artificially attach a trailer to collected car data without trailer. The framework would allow evaluating TPI functionality in the scenario of having a trailer connected to a car, by modifying collected test data logs where no trailer actually was connected.

1.4 Demarcation

In this thesis, the wheel radii monitoring subsystem of TPI is of more interest than the frequency monitoring subsystem. Further, due to legal requirements of towing trailers in Sweden, no higher velocities than 80 km/h should be required to be captured in the model. For the purposes of evaluating TPI performance, high lateral accelerations or braking are considered out of the scope for this project.

1.5 Pre-study and planning

An initial pre-study and planning phase was performed. The pre-study consisted of researching related work, mainly car- and car-trailer system dynamics modeling. The planning phase included writing a project plan with a SWOT risk analysis, and constructing a Gantt scheme with milestones and tollgates. The Gantt scheme was evaluated on a regular basis for the duration of the project.

1.6 Related work

There are many dynamical models for car-trailer systems described in the literature, often with focus on different aspects of the system as well as with varying complexity [4], [5], [6], [7], [8]. Among others there are simple linear models with few degrees of freedom (DOF) such as the linear 3DOF model proposed by Ellis [9], more complex nonlinear models such as the 4DOF and 6DOF models proposed by Anderson and Kurtz [10], as well as highly complex high DOF nonlinear multibody simulation models in software tools such as ADAMS car [11]. Since the car-trailer system is susceptible to loosing directional steering capability and stability, a large portion of research in car-trailer system dynamics focuses on the lateral dynamics.

Wong [12] summarized a comparison between state estimations from four different car-trailer system models with corresponding experimentally gathered measurement data. These system models were a linear yaw-plane model, a nonlinear yaw/plane model named TBS, a nonlinear yaw-roll model and a nonlinear high DOF model called Phase 4. The conclusion was that up to $0.25g$, there were no significant differences in steady-state steering. There was however a significant difference between the linear yaw plane model and the other nonlinear models when comparing vehicle handling in the lateral direction. This was due to the linear model neglecting load transfer and assuming linear tire dynamics - which the other models all incorporate to varying extent.

He and Ren [13] made a similar comparative study, but instead of using experimental data as reference they used the CarSim simulation software which is built on a nonlinear 21 DOF model. Similar results for a linear yaw plane model were obtained, proving effective at lateral stability estimation only as long as the lateral acceleration were below $0.3g$. Neglecting the lateral tire force saturation was regarded as the reason for this limitation.

They further showed that a 6DOF nonlinear yaw-roll model, which included lateral tire force saturation and load transfer, could instead be used to achieve high fidelity even during high lateral accelerations.

The choice of model type depends on its intended use. While complex models in general offer more realistic estimates, the amount of required input data to the model as well as parameters needed to be estimated has to also be considered. An illustrative example of this was given by Wong [12], where the linear yaw/plane model only required about 35 lines of input data, while the Phase 4 model required up to 2300 lines of input data.

1.7 Ethics in the automotive industry

The Institute of Electrical and Electronics Engineers (IEEE) have general codes of conduct that an engineer is expected to uphold and can use as guidance [14]. These include to uphold high standards of integrity in various ways, to treat all human beings with respect and to help other engineers to also follow these codes of ethics. However, these guidelines have been suggested to not completely cover all the specific issues and dilemmas a robotics engineer could be expected to face [15], [16]. As personal vehicles are becoming more intelligent, autonomous and connected, this is highly relevant for engineers working in the automotive industry.

Ingram et.al. therefore suggest a code of ethics tailored specifically for robotics engineers [15]. They focus on the fact that as robotics systems reach higher levels of autonomy, engineers also must think proactively about and take responsibility for the future actions taken by their creations. They also call upon the robotics engineers to take responsibility of how their creations contribute, among other things, to the well-being of the local people and environment, the expectations and safety of the customer as well as the reputation and economic situation of the employer.

Veruggio and Operto suggest 'Roboethics' [16] as a type of applied ethics, concerning the ethical issues that might arise specifically in the design, development and employment of intelligent machines. They propose a process of how to debate and decide on robotics ethics, either by technical experts or by society as a whole, depending on what type of issue is at hand. Common to all these guidelines and philosophies is the message that engineers as a group have a large responsibility in recognizing both potential harm and benefits of their actions, and that they should do their utmost to minimize conceivable harm to their communities. This master thesis aims to achieve reliable and trustworthy simulation results. Ethics had to be considered regarding the safety of using simulations rather than in-vehicle tests, but also regarding the ultimate goal of making driving more safe, economic and environmentally friendly.

Chapter 2

Parameter identification and model analysis

In this chapter, signal processing concepts and algorithms used for parameter estimation and frequency analysis are described. First, the multivariate normal distribution is defined in Section 2.1. The results will be used for some of the performance evaluation criterion in the hybrid simulations. Then, the method of least squares is described in Section 2.2 as a way to estimate unknown parameters. Finally, the procedure to compute the natural frequencies of a linear system is shown in Section 2.3.

2.1 Multivariate normal distribution

A multivariate normal distribution of order D is defined as

$$\mathbf{x} \sim \mathcal{N}(\mu, \mathbf{\Sigma}) \tag{2.1}$$

where $\mu \in \mathcal{R}^D$ is the mean and $\mathbf{\Sigma} \in \mathcal{R}^{DxD}$ is the covariance matrix [17]. Its probability density function is given by

$$\mathcal{N}(\mu, \mathbf{\Sigma}) = \frac{1}{(2\pi)^{\frac{D}{2}}} \frac{1}{|\mathbf{\Sigma}|^{\frac{1}{2}}} \exp\left(-\frac{1}{2}(\mathbf{x}-\mu)^T \mathbf{\Sigma}^{-1}(\mathbf{x}-\mu)\right), \tag{2.2}$$

where $|\mathbf{\Sigma}|$ is the determinant of Σ. One can see that it is only the exponential term of (2.2) that is not a constant. Therefore, giving the exponential term a variable name of its own as

$$\Delta^2 = \frac{1}{2}(\mathbf{x}-\mu)^T \mathbf{\Sigma}^{-1}(\mathbf{x}-\mu), \tag{2.3}$$

it is more clearly seen that the distribution will have constant probability density on surfaces where Δ^2 is constant. To describe these constant density surfaces, a distance measure is needed. The generalization from the univariate case of how far away a point $\mathbf{x} \in \mathcal{R}^D$ is from a distribution mean μ is exactly Δ, which is called the Mahalanobis distance [18]. To see this, one can search for the eigenvectors u_i of the covariance matrix by

$$\mathbf{\Sigma}\mathbf{u}_i = \lambda_i \mathbf{u}_i, \tag{2.4}$$

where $i = 1, .., D$. Due to the symmetric properties of $\mathbf{\Sigma}$, it can be expressed as

$$\mathbf{\Sigma} = \sum_{i=1}^{D} \lambda_i \mathbf{u}_i \mathbf{u}_i^T, \tag{2.5}$$

and similarly its inverse

$$\mathbf{\Sigma}^{-1} = \sum_{i=1}^{D} \frac{1}{\lambda_i} \mathbf{u}_i \mathbf{u}_i^T. \tag{2.6}$$

Substituting $\mathbf{\Sigma}^{-1}$ into (2.3), taking the square root on both sides, one arrives at

$$\Delta = \sum_{i=1}^{D} \frac{y_i}{\sqrt{\lambda_i}}, \tag{2.7}$$

where

$$y_i = \mathbf{u}_i^T (\mathbf{x} - \mu). \tag{2.8}$$

For $D = 2$, Equation (2.7) takes the form of the standard equation of an ellipse with semi axes of length $\sqrt{\lambda_1}$ and $\sqrt{\lambda_2}$ in a new coordinate system defined by y_1 and y_2. The new coordinate system will be shifted and rotated relative the original x axes, see Figure 2.1. The ellipse axes lengths are scaled by Δ, which as described above, is the natural distance measure from the mean of the distribution.

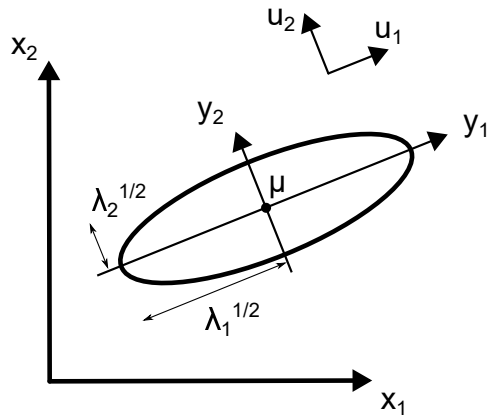

Figure 2.1 – Gaussian confidence ellipse, drawn with $\Delta = 1$ so that the semi axes lengths are equal to $\sqrt{\lambda_1}$ and $\sqrt{\lambda_2}$.

It can be shown that Δ^2 for a multivariate normal distribution of degree D follows a χ^2 distribution of D degrees of freedom [19]. This means that Δ can be computed by evaluating the inverse χ^2 distribution at D degrees of freedom up to any desired confidence value and then be used to determine the semi-major and semi-minor axes lengths for any desired confidence contour ellipse (for example the commonly used 68% or 95% confidence intervals). For $D = 1$, the results reduce to the familiar univariate case where the probability of observing a sample within $\mu \pm \sigma$ is approximately 68.27 %, but for any higher dimension the probability of observing a sample in the same interval would be lower [19].

This is why it is important to compute the Mahalanobis distance from the appropriate order D and scale the eigenvalues with this value instead of just the number of desired standard deviations as one can do in the univariate case.

2.2 Least squares

Consider a discrete linear model with output $y(i)$ of the form

$$y(i) = \phi^T(i)\theta, \tag{2.9}$$

where

$$\phi^T(i) = \begin{bmatrix}\phi_1(i) & \phi_2(i) & \dots & \phi_n(i)\end{bmatrix} \tag{2.10}$$

is a column vector of n known functions and

$$\theta(i) = \begin{bmatrix}\theta_1(i) & \theta_2(i) & \dots & \theta_n(i)\end{bmatrix}^T \tag{2.11}$$

is a column vector of n unknown coefficients to be estimated. The most common method to estimate the parameters θ is by the principle of least squares. The method minimizes the errors of the estimated output, where the errors are defined as the squared sum of the estimated output differences. More formally, this is equivalent of saying that one should minimize the loss function

$$V(\theta, t) = \frac{1}{2}\sum_{i=1}^{t}\left(y(i) - \phi^T(i)\hat{\theta}\right)^2, \tag{2.12}$$

where $\hat{\theta}$ is the estimated parameters. It can be shown [20] that (2.12) is minimal for $\hat{\theta}$ when

$$\Phi^T\Phi\hat{\theta} = \Phi^T Y, \tag{2.13}$$

where

$$Y(t) = \begin{bmatrix}y(1), & y(2), & \dots & y(t)\end{bmatrix}^T \tag{2.14}$$

and

$$\Phi(t) = \begin{bmatrix}\phi^T(1)\\ \phi^T(2)\\ \vdots\\ \phi^T(t)\end{bmatrix}. \tag{2.15}$$

Further, for nonsingular $\Phi^T\Phi$, the minimal estimates are found when

$$\hat{\theta} = (\Phi^T\Phi)^{-1}\Phi^T Y. \tag{2.16}$$

2.3 Natural frequencies of a spring-mass system

For a spring-mass system

$$\mathbf{M}\ddot{\mathbf{x}} + \mathbf{K}\mathbf{x} = \mathbf{0} \tag{2.17}$$

the eigenvalues λ are given by solving the characteristic equation

$$\det(\mathbf{K} - \lambda\mathbf{M}) = \mathbf{0}. \tag{2.18}$$

Each eigenvalue is directly related to a natural frequency ω_n of the system by the relation [12]

$$\omega_n = \sqrt{\lambda}. \tag{2.19}$$

Chapter 3

Models

In this chapter, mathematical models of the car-trailer system dynamics are described. First, vehicle dynamics necessary to describe the car and trailer are covered in Section 3.1. Then, the major forces acting on a car-trailer system are explained in Section 3.2. Based on these forces, a planar Force model is derived. This model was developed in order to be able to compute the forces acting on the car and car-trailer system from sensor signals.

The outputs cover all the major physical phenomena which the project intended to investigate. The vertical vibration dynamics are not captured in this model however. Due to this, a 3DOF model describing the vertical dynamics of the car-trailer system is derived in Section 3.3, allowing for study of the natural frequencies of the system. This model was used as a theoretical ground to compare the frequency spectra of the gathered data against.

3.1 Vehicle Dynamics

In this section, some of the fundamentals of vehicle dynamics are described. To describe the motion of a car, an axis system for the car is needed. The standard axis system for a car in the automotive industry [21] is drawn in Figure 3.1. The yaw, pitch, and roll angles of rotation are also shown.

Figure 3.1 – Standard car axis system.

3.1.1 Tires

Apart from the gravitational and aerodynamic forces, the most important forces and moments describing the dynamics of a ground vehicle are concentrated at the vehicle tires. In order to describe these forces and moments, it is common to use the specific standard axis system for tires proposed by the Society of Automotive Engineers, as shown in Figure 3.2.

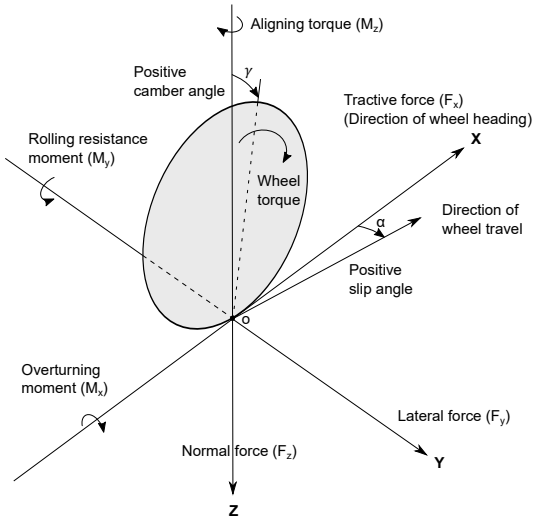

Figure 3.2 – Tire axis system.

Among the three forces and three moments acting on the tire, it is shown that the tractive force F_x is the component of the force exerted by the tire on the road that lies in the x direction (wheel heading). One can also see that rolling resistance is drawn as a moment. This is due to the rolling resistance being mainly caused – not by friction between tire and ground – but by hysteresis losses in the tire. As the tire rolls forward, the front of the tire deflects at the ground contact surface due to its elastic materials.

The deflection leads to a shift in the tire normal pressure towards the direction of rolling. This shift in normal pressure gives rise to a moment about the wheel axis, which is what is referred to as the rolling resistance moment. When the tire keeps rolling the deflected part of the tire recovers, but the energy lost due to its deformation is larger than the energy of recovery, resulting in hysteresis.

By using the proposed coordinate system, the rolling resistance coefficient f_{rr} can be derived as the ratio of the rolling resistance force to the normal load. Apart from being dependent on structure and materials of the tire, the coefficient also depends on varying parameters such as surface conditions, inflation pressure, speed and temperature.

Due to the complex nature of all factors contributing to the rolling resistance, it is common to rely on experimentally gathered data to model it during different driving conditions. For instance, a commonly used [22] average value of f_{rr} for passenger cars on concrete and asphalt is

$$f_{rr} = 0.013. \tag{3.1}$$

There are also other models capturing the velocity dependence of the rolling resistance with a small term proportional to the square of the velocity. Under conditions of rated loads and

inflations, as well as hard, smooth and flat road, one such model is

$$f_{rr} = 0.0136 + 0.40\ 10^{-7} v^2, \tag{3.2}$$

where v is in km/h [22].

3.1.2 Longitudinal slip

The relative motion between the road and the driven tire tangential speed is referred to as longitudinal slip, i, and can be formulated as

$$i = \frac{\omega r - v}{v} \cdot 100\%, \tag{3.3}$$

where v is the linear speed of the tire center, r is the tire radius in free rolling and ω is the angular speed of the tire. An illustrative case resulting in infinite slip could be when a car is trying to drive on ice but not managing to move forward, its driven wheels spinning in place.

For tractive forces up to approximately $\frac{\mu_p W}{2}$, the tractive force can be regarded as increasing linearly with the slip [12]. This is due to the slip in this region being mainly caused by the elastic materials in the tire compressing. Here, μ_p represents the peak value of the coefficient of road adhesion, and W the normal force of the vehicle. For larger values of slip, the tire begins to slide on the surface, resulting in a nonlinear relationship up to the maximum possible tractive force $\mu_p W$.

After this, the tractive force decreases to finally reaching a maximum slip at $\mu_s W$, where μ_s is the sliding value of the coefficient of road adhesion. The relationship between slip and traction force is often approximated with the empirical "Magic Formula" by Pacejka [23], qualitatively illustrated in Figure 3.3 with regions of interest marked. The approximately linear relationship up to a traction force of $\mu_p \frac{W}{2}$ can be seen.

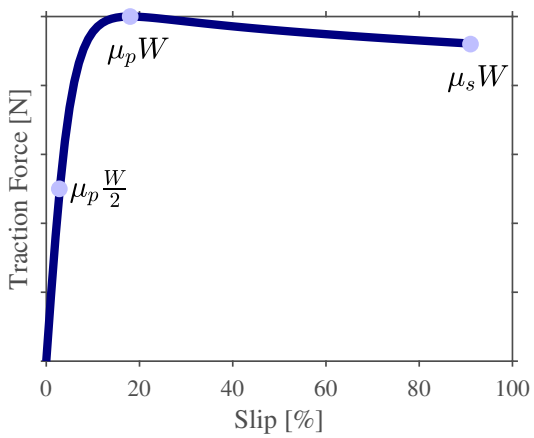

Figure 3.3 – Slip and traction force relationship by the Magic Formula.

3.1.3 Traction force

The traction force F_x exerted by the driven wheels on the ground can be modeled as

$$F_x = \frac{M_e \xi_0 \eta_t}{r}, \tag{3.4}$$

where M_e is the engine output torque, ξ_0 is the overall reduction ratio of the transmission, η_t the overall transmission efficiency, and r is the driving wheel radii [12]. One can relate ξ_0 to the ratio of engine to vehicle speed by

$$\xi_0 = \frac{n_e}{\omega_F}(1 - i), \tag{3.5}$$

where n_e and ω_F are the engine and wheel angular velocities respectively and i the longitudinal slip [12].

3.1.4 Aerodynamics

A common model of air resistance [12] R_a is

$$R_a = \frac{\rho}{2} C_d A_f v^2, \tag{3.6}$$

where ρ is air density in $\frac{kg}{m^3}$, C_d is a dimensionless aerodynamic constant of the system, A_f the frontal area of system in m^2 and v the linear velocity of the system relative wind in $\frac{m}{s}$.

3.2 Force model

The forces acting on a car-trailer system can be modeled and illustrated as shown in Figure 3.4.

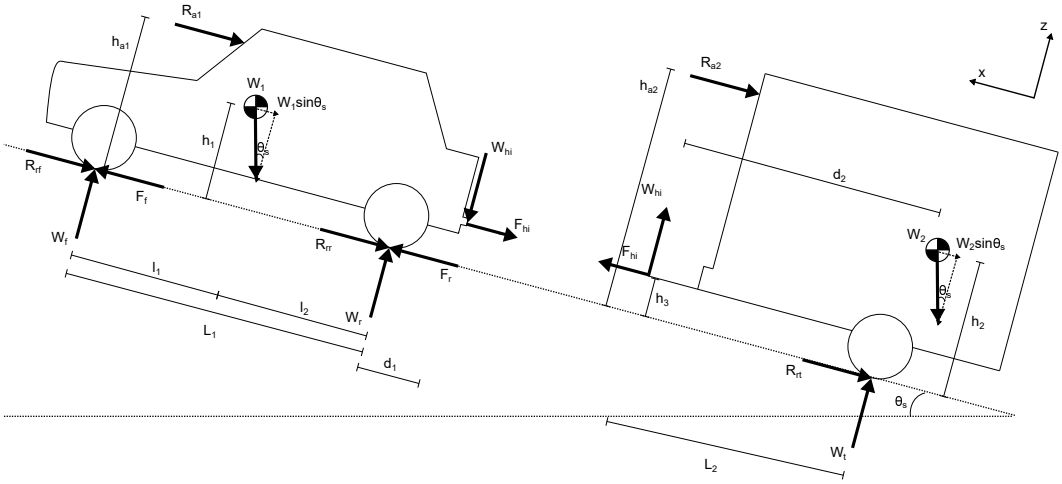

Figure 3.4 – Car with trailer attached, forces acting on the the two sub systems drawn.

These forces include the tractive effort F_f and F_r of the front and rear tires, the rolling resistance of the tires R_{rf}, R_{rr}, R_{rt}, the aerodynamic resistance R_{a1} and R_{a2} due to the

car and trailer moving, the weights W_1 and W_2 of the car and trailer, the normal forces at each tire pair W_f, W_r, W_t, and the vertical and horizontal load at the hitch W_{hi}, F_{hi}. A grade resistance $R_{\theta_s} = W \sin(\theta_s)$ is introduced if the system is driving at a slope, where $\theta_s > 0$ if the slope is uphill and $\theta_s < 0$ if the slope is downhill.

By summing forces and moments in figure 3.4, rearranging for variables of interest, one obtain the expressions that describe the system dynamics as

$$a_x = \frac{g}{W_1 + W_2}(F_f + F_r - R_{a1} - R_{a2} - R_{rf} - R_{rr} - R_{rt} - (W_1 + W_2)\sin\theta_s), \tag{3.7}$$

$$W_t = \frac{1}{L_2}((h_{a2} - h_3)R_{a2} + (h_2 - h_3)W_2 \sin\theta_s + d_2 W_2 \cos\theta_s + (h_2 - h_3)\frac{W_2}{g}a_x - h_3 R_{rt}), \tag{3.8}$$

$$W_{hi} = W_2 \cos\theta_s - W_t, \tag{3.9}$$

$$F_{hi} = \frac{W_2}{g}a_x + R_{rt} + R_{a2} + W_2 \sin\theta_s, \tag{3.10}$$

$$W_r = \frac{1}{L_1}(l_1 W_1 \cos\theta_s + h_{a1}R_{a1} + h_1 W_1 \sin\theta_s + h_1 \frac{W_1}{g}a_x + (L_1 + d_1)W_{hi} + h_3 F_{hi}), \tag{3.11}$$

and

$$W_f = \frac{1}{L_1}(l_2 W_1 \cos\theta_s - h_3 F_{hi} - d_1 W_{hi} - h_{a1}R_{a1} - h_1 \frac{W_1}{g}a_x - h_1 W_1 \sin\theta_s). \tag{3.12}$$

3.3 Pitch-Bounce model

A Pitch-Bounce model was derived in order to investigate trailer dependent frequency content. The model included axle suspensions and a longitudinally adjustable trailer load. A free body diagram of the system is shown in Figure 3.5.

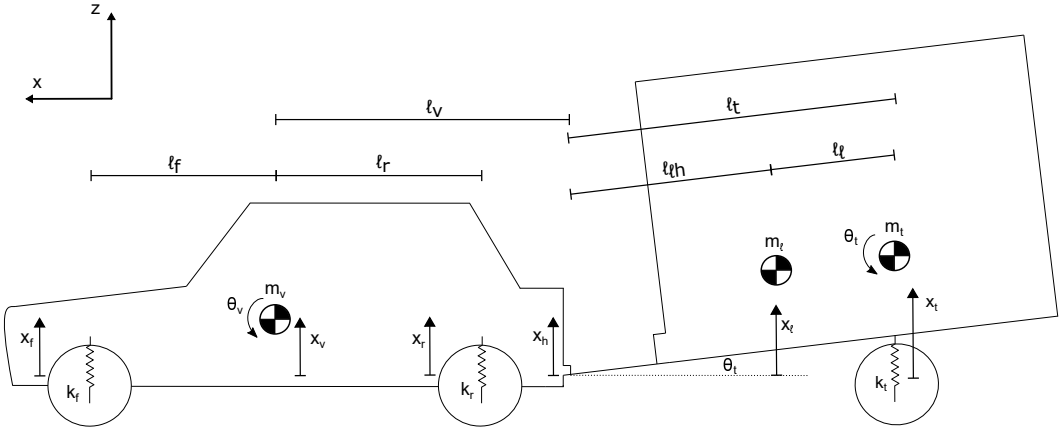

Figure 3.5 – Free body diagram of a trailer with load attached to car, including suspensions for both vehicles.

The following derivation of the system dynamics in Figure 3.5 uses small angle approximations for the angles θ_v and θ_t so that a linearized model is obtained. The forces acting on the system can be expressed as

$$F_f = -k_f x_f = -k_f(x_v - \ell_f \theta_v), \tag{3.13}$$

$$F_r = -k_r x_r = -k_r(x_v + \ell_r \theta_v), \tag{3.14}$$

$$F_\ell = -m_\ell \ddot{x}_\ell = -m_\ell(\ddot{x}_t - \ell_\ell \ddot{\theta}_t), \tag{3.15}$$

and

$$F_t = -k_t x_t. \tag{3.16}$$

By summing forces and moments about both the car and trailer CoG, one arrives at

$$m_v \ddot{x}_v = F_f + F_r + F_h, \tag{3.17}$$

$$I_v \ddot{\theta}_v = -F_f \ell_f + F_r \ell_r + F_h \ell_{vh}, \tag{3.18}$$

$$m_t \ddot{x}_t = F_t - F_h + F_\ell \tag{3.19}$$

and

$$I_t \ddot{\theta}_t = F_h \ell_t - F_\ell \ell_\ell. \tag{3.20}$$

The vertical displacement of the load x_ℓ can be expressed as

$$x_\ell = x_t - \ell_l \theta_t, \tag{3.21}$$

and similarly the vertical displacement of the hitch x_h as

$$x_h = x_v + \ell_{vh} \theta_v \tag{3.22}$$

resulting in the expression for the trailer angle

$$\theta_t = \frac{x_t - x_h}{\ell_t} = \frac{x_t - (x_v + \theta_v \ell_{vh})}{\ell_t}. \tag{3.23}$$

Proceeding, it is possible to eliminate $\ddot{\theta}_t$ in the force and moment equations by differentiating (3.23) twice such that

$$\ddot{\theta}_t = \frac{\ddot{x}_t - \ddot{x}_v - \ddot{\theta}_v \ell_{vh}}{\ell_t}. \tag{3.24}$$

Substituting (3.23) into the force and moment equations, one finally arrives at the equation system

$$\begin{cases} m_v \ddot{x}_v + k_f(x_v - \ell_f \theta_v) + k_r(x_v + \ell_r \theta_v) - F_h = 0, \\ I_v \ddot{\theta}_v - k_f(x_v - \ell_f \theta_v)\ell_f + k_r(x_v + \ell_r \theta_v)\ell_r - \ell_{vh} F_h = 0, \\ m_t \ddot{x}_t + k_t x_t + m_\ell(\ddot{x}_t - \frac{\ell_\ell}{\ell_t}(\ddot{x}_t - \ddot{x}_v - \ddot{\theta}_v \ell_{vh}) + F_h = 0, \end{cases} \tag{3.25}$$

with

$$F_h = \frac{1}{\ell_t^2}\left((I_t + m_\ell \ell_\ell^2)(\ddot{x}_t - \ddot{x}_v - \ddot{\theta}_v \ell_{vh}) - \ell_t m_\ell \ell_\ell \ddot{x}_t\right). \tag{3.26}$$

These system equations in (3.25) can be arranged in matrix form as

$$\mathbf{M}\ddot{\mathbf{x}} + \mathbf{K}\mathbf{x} = \mathbf{0} \tag{3.27}$$

with

$$\mathbf{x} = \begin{bmatrix} x_v \\ \theta_v \\ x_t \end{bmatrix}. \tag{3.28}$$

The system can be completely described by the three state variables in (3.28). This means that frequency analysis of the corresponding linear system will result in three eigenfrequencies, also completely characterizing the system. Eliminating other state variables than $\ddot{\theta}_t$ would hence be possible but unnecessary for these purposes since it would not result in any other eigenfrequencies.

Chapter 4

Data gathering and computations

In this chapter, the data gathering and following vehicle dynamics computations and estimations on the gathered data are presented. Experiment planning and data gathering are described in Section 4.1. Vehicle dynamics computations are described in Section 4.2. Section 4.3 describes parameter estimations for the Force and Pitch-Bounce models.

4.1 Data gathering

Any model of a real life system needs to be evaluated and verified on experimentally gathered data. For physical modeling there are often parameters to be estimated or identified that are unique for the particular system in question as well. For these reasons there were a need to gather car-trailer data.

Sensors and sensor signals available in the experiment car, Audi A6 Avant 2020, included accelerometer, wheel encoders, motor torque, high performance GPS (including altitude) and axle height sensors on front and rear axis. All sensors were sampled with at least 10 Hz. Approximate wind speeds were documented after the experiments were performed, with data from available wind stations nearby [24].

The car and trailers used are shown in Figures 4.1, 4.2, 4.3 and 4.4.

(a) Front view.

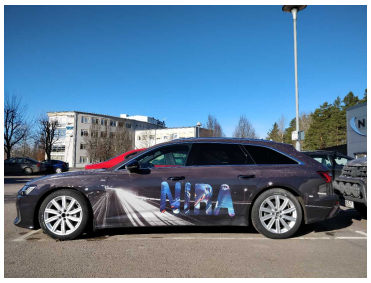

(b) Side view.

Figure 4.1 – The car used in the experiments, Audi A6 Avant 2020.

(a) Front view.

(b) Side view.

Figure 4.2 – Small trailer with one axis.

(a) Front view.

(b) Side view.

Figure 4.3 – Medium trailer with two axes.

(a) Front view.

(b) Side view.

Figure 4.4 – Large trailer with three axes.

The dimensions and parameters of the car (including two persons in the front seats) are shown in Table 4.1.

Table 4.1 – Dimensions and parameters for Audi A6 Avant with two persons in front seats.

Car dimensions		
Parameter	**Audi A6 Avant 2020**	**Source**
L_1 $[m]$	2.933	Measured
l_1 $[m]$	1.349	Measured
l_2 $[m]$	1.584	Measured
d_1 $[m]$	1.222	Measured
m $[kg]$	2039	Measured
h_1 $[m]$	0.489	Assumption
h_{a1} $[m]$	0.632	Assumption
C_D $[-]$	0.28	Datasheet (Audi)
A_f $[m^2]$	2.33	Datasheet (Audi)

For the vertical height of applied aerodynamic resistance h_{a1}, it was assumed that the force could be regarded as applied at the middle of the front height of the car. The car vertical CoG was assumed to be located at a third of the known (from datasheet) total height of the car, making $h_a = \frac{1.467}{3} = 0.489$.

The dimensions and parameters of the trailers are detailed in Table 4.2. As no typical C_D for these types of trailers could be found in previous work during the project, the full typical C_D ranges for vans ([0.4-0.58]) and buses ([0.5-0.8]) [12] were used as initial guesses instead.

Table 4.2 – Dimensions and parameters for the trailers.

Trailer dimensions				
Parameter	**Small trailer**	**Medium trailer**	**Large trailer**	**Source**
L_2 $[m]$	2.66	2.92	4.02	Measured
d_2 $[m]$	2.51	3.13	4.04	Measured
m $[kg]$	252	631	1389	Measured
h_3 $[m]$	0.5	0.37	0.57	Measured
h_2 $[m]$	0.6	0.47	0.67	Assumption
h_{a2} $[m]$	0.8	1.0	1.05	Assumption
C_D $[-]$	0.4	0.6	0.8	Assumption
A_f $[m^2]$	1.80	3.42	4.53	Measured

In order to separate the forces resulting from driving a car with a trailer attached, different data gathering scenarios were constructed. Since no lateral dynamics were to be modeled in this project, any lateral dynamics were considered as disturbances and thus effort was spent to minimize these effects. To highlight trailer effect further, a pallet load with mass 403 kg was put in the Small trailer in front, mid (above trailer wheel axis) and rear position, see Figure 4.5. In order to effectively move the load inside the trailer at the test sites without going back to the garage, a pallet jack was used, which increased the load weight by 48.5 kg to a total weight of 451.5 kg.

(a) Pallet in garage trailer tests.

(b) Pallet and pallet jack during driving tests.

Figure 4.5 – Load inside Small trailer.

4.1.1 Weighing of car and trailers

Before any driving tests were performed, the car and trailers were weighed using four scales placed under each vehicle in appropriate settings. The weighing experiments were performed inside in a garage on flat concrete floor. By summing each scale measurement, a total mass estimate of each vehicle was obtained. In addition, each vehicle center of gravity (CoG) could be estimated by utilizing the individual scale measurements in combination with known lengths of each vehicle.

Besides individual vehicle weighing experiments, weighings of the car with the Small trailer attached were also performed. During these tests, the Small trailer was loaded with a 403 kg pallet and moved between mid, rear and front trailer positions. During these experiments, data from the car front and rear axle height sensors were gathered. Since the different loading scenarios of the trailer would either lift or lower the car axes, the relationship between car axis height and car axis normal force could be observed. The experimental setup is shown in Figure 4.6.

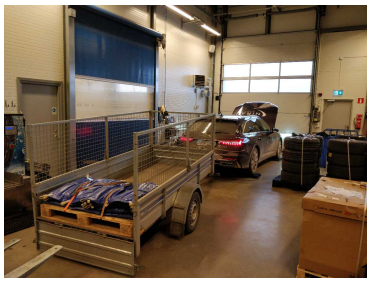

(a) Rear loaded trailer attached.

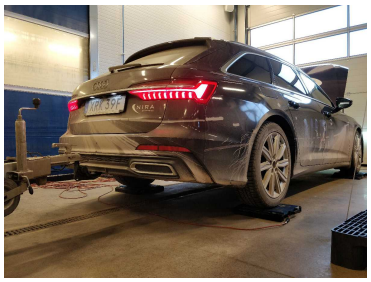

(b) Scales under each car tire.

Figure 4.6 – Experiment to observe relationship between car axis heights and normal forces.

Individual vehicle weighings are shown in Table 4.3, where mean front and rear axis weights have been computed by taking the mean of the left and right scale for each axis. From the weighings, CoG for each vehicle was computed.

Table 4.3 – Weighing results.

Weighing results			
Vehicle	**Front axis [kg]**	**Rear axis [kg]**	**Total [kg]**
Audi A6 Avant	1012	858	1869
Small trailer	222	31	252
Medium trailer	470	162	631
Large trailer	1368	21	1389

The experiment showing the relationships between car axis height and its respective normal force is shown in Figure 4.7. Since the relationships were so linear, first order approximations were made for the front and rear axle height to normal force relationships, parameterized by parameters p_F and p_R. This enabled the axle height sensors to provide reference values for the normal forces computed by the Force model while driving.

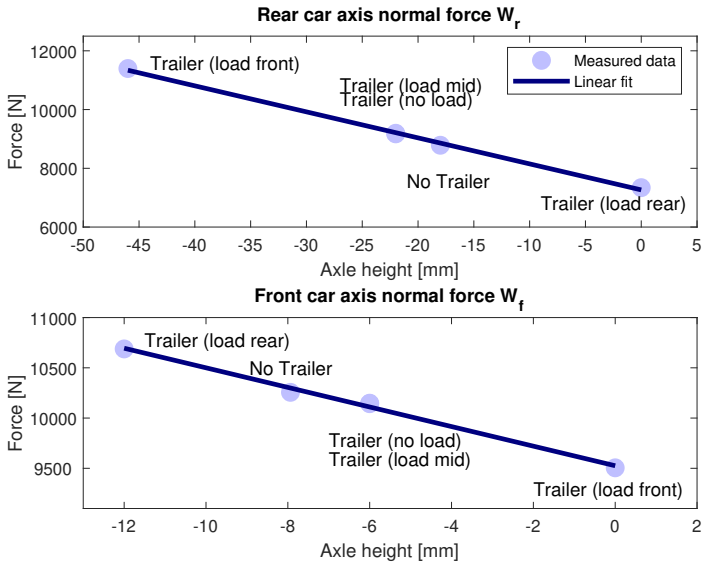

Figure 4.7 – Axle height to normal force garage experiment.

4.1.2 Rolling and aerodynamic resistance experiment

For the longitudinal dynamics, rolling and aerodynamic resistance were the main resistive forces expected to influence the system. To isolate these forces, test scenarios on a flat, straight road were formulated. Since the road was straight and flat, the influence of lateral dynamics and grade resistance would be kept to a minimum.

To further separate the rolling resistance from the aerodynamic resistance, an evenly spaced range of velocities in the range 35, 50, 65 and 80 km/h were specified.

These velocities were to be kept approximately constant at four corresponding distance slots of equal length along the road. The idea was that since the aerodynamic resistance depends on velocity squared, while the rolling resistance can be modeled as a constant or at most as having a very small velocity dependence, the resistive forces would be separable. The maximum speed was set to 80 km/h due to it being the highest allowed driving speed

with trailer attached in Sweden. The lower limit of 35 km/h was set due to safety reasons so as to not disturb regular traffic too much. Further safety aspects were considered as the road in addition to previously mentioned criterion should preferably have both 2 lanes to enable overtaking, max 80 km/h speed limit to enable all speed slots and low traffic activity to reduce traffic disturbance due to low speed driving.

The road segment also had to be somewhat close to the NIRA Dynamics AB garage in Linköping since the vehicles were all stationed there. A road fitting these criterion was found between the urban areas Klockrike and Fornåsa. It had a 5.0 km, straight and flat, 0.06 deg (0.10 %) average slope, low traffic, two lane, max 80 km/h stretch, fitting the needs of this project. To somewhat compensate for wind direction as well as increase data amount, the tests were made in both directions. The four speed slots were driven in ascending order in one direction and descending order in the opposite direction.

In addition to the speed slot tests, coastdown tests were also performed. A coastdown test is a well known method of experimentally determining rolling resistance, aerodynamic resistance and driveline resistance [12], [25]. It is performed by accelerating the vehicle on a straight and flat road to a certain speed and then letting it roll with the engine disengaged until it stops [26]. These methods are standardized under among others SAE J1263. Some relevant technical specifications in SAE J1263 are speed ranges of 40-100 km/h, track slope < 0.5 %, wind speed 20 km/h (approximately 5.56 m/s), tire pressure at manufacturer's specification and test track "Sufficiently long and straight" [26]. FCA 7-T3040 (Ref. SAE J1263) has similar specifications, specifying speeds up to 140 km/h, wind speeds < 2m/s and test track of 2000 m.

For the purposes of this project towing trailers, no speeds higher than 80 km/h were possible due to legal reasons, making it impossible to completely fulfill either specification, but still deemed to be the best possible approach available. In addition, according to ISO 8767 a tire should be run about 20 min before every measured speed [27]. Pure acceleration and braking tests were also performed with all vehicles combinations. The system was accelerated from standstill to 80 km/h, and then brought to a halt by braking. Both acceleration and braking were done in a more aggressive than standard driving manner. These tests were performed in order to evaluate model performance on more extreme conditions as well as highlighting longitudinal slip.

To investigate grade resistance effects on the car-trailer system a long, straight and as steep as possible slope was required. A slope with an average of 1.25 deg (2.18 %) over 2400 m near Borensberg was used for this experiment. To isolate grade resistance from traction force, the vehicle was let roll with the gear in neutral down the steepest part of the slope in a coastdown test fashion.

The performed driving tests and their corresponding conditions are shown in Table 4.4. Compensations were made by simulating a constant wind vector with magnitude and direction from available observed data after the experiment. This made it possible to reduce large parts of the residual error offset that otherwise occured after turning around and driving back to the route starting point.

For route type "Straight and flat", speed slot tests, acceleration tests, braking tests and coastdown tests were performed. For route type "Slope", constant speed test and coastdown in slope were performed.

Table 4.4 – Test scenarios performed. The Audi A6 Avant was used in the towing of the trailers.

Test scenarios			
Vehicle	**Route**	**Trailer load [kg]**	**Trailer load position**
Audi A6 Avant	Flat	-	-
	Slope	-	-
Small trailer	Flat	451.5	Mid
	Flat	451.5	Front
	Flat	451.5	Rear
	Slope	451.5	Mid
	Slope	451.5	Front
	Slope	451.5	Rear
Medium trailer	Flat	0	-
	Slope	0	-
Large trailer	Flat	0	-
	Slope	0	-

4.1.3 Data gathering summary

Summarizing the data gathering, focus is directed to the Small trailer due to it being the only trailer with additional load inside so that the effects of longitudinal load transfer could be shown. Results from the Medium and Large trailer are also shown, with highlights where the larger size and weight result in significant output differences. Numerical results are given in tabular form for all trailers and driving routes. The wind speeds at the time intervals of data gathering are shown in Table 4.5.

Table 4.5 – Wind situation during the four days of data gathering.

Wind situation				
Trailer	**Route**	**Date**	**Wind vel** $[\frac{m}{s}]$	**Wind bearing**
Small	Flat	2021-02-26	9	W
Small	Slope	2021-03-22	8	W
Medium	Flat	2021-03-23	4.5	W-SW
Medium	Slope	2021-03-23	4.5	W-SW
Large	Flat	2021-03-01	8	SW
Large	Slope	2021-03-01	8	SW

The normal force model estimates are put in relation to the normal forces computed from axle height in Figure 4.8. The Force model generally showed good consistency with the normal forces computed from the axle height sensors.

The typical characteristic of the longitudinal slip i in relation to the tractive effort is shown in Figure 4.9. The trailer load position dependency can be seen in all plots by the offset separation of each point cloud. In the top plots, the offset is vertical. In the bottom plots, the offset is mainly horizontal. The top plots show that the rear loaded trailer causes more slip at the same traction force than the mid and front loaded trailer.

This makes sense, since a rear loaded trailer would apply a larger force at the car hitch,

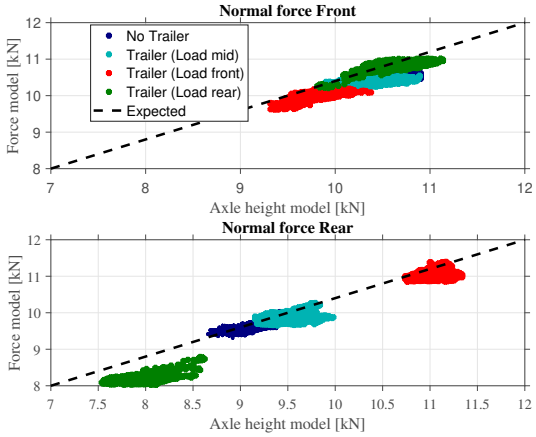

Figure 4.8 – Normal force model compared to the estimates from axle height. The dashed line show what the relationship should look like if the two models output identical estimates.

causing the car front axle to rise, effectively reducing the front wheel normal forces. The front and rear normal forces illustrate this in the bottom plots by the not only varying slip but also offsets in normal force between the data sets.

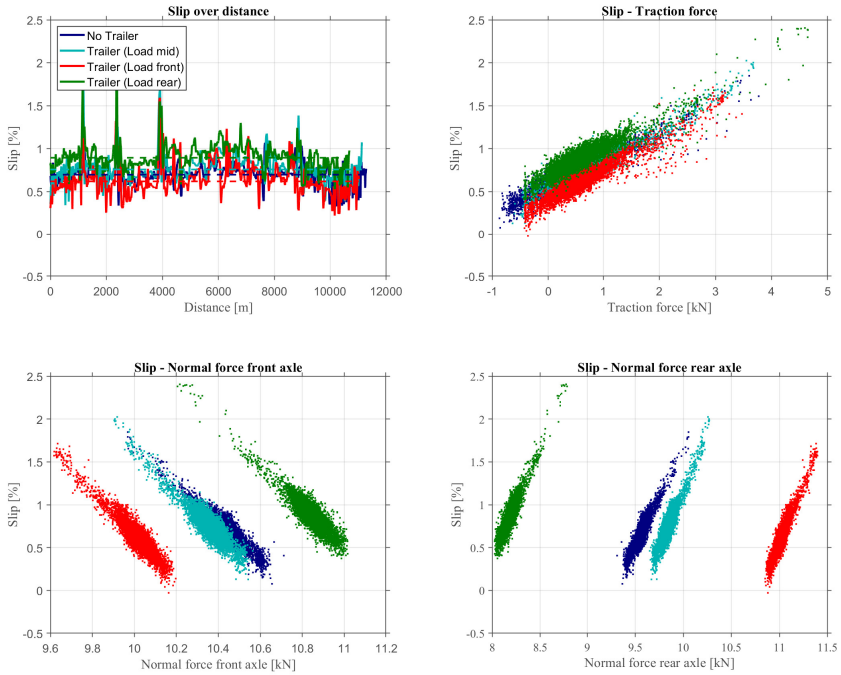

Figure 4.9 – Longitudinal slip, Small trailer attached, Flat route. In the top left plot, slip is shown varying over time. In the top right plot, it is plotted against traction force. In the bottom plots, slip is plotted against the car front and rear axle normal forces.

4.2 Vehicle dynamics computations from gathered data

In this section the computations performed on the gathered sensor data is explained. Some of the gathered data was noisy and had to be smoothed out before use in the computations. Moving mean filters with a window size of 15 samples where used to smooth the noisy accelerometer, front and rear axle height signals as well as the differentiated wheel speed signals and computed slope angles. The main computations are shown in the following subsections.

4.2.1 Traction force

The traction force F_x for the front-driven automatic transmission Audi A6 Avant was estimated by means of available sensor signals and computed as derived in Equation (3.4). First, the engine-to-wheel gear ratio ξ_0 was estimated from the front wheel angular velocities ω_F obtained from odometry sensors and measured engine speed n_e.

Some standard assumptions were made for the energy losses between the motor torque and the front wheel traction force. The slip i was assumed a constant 1 % and the overall transmission efficiency η_t was set to 0.9310, stemming from assuming a gearbox and drive axle mechanical efficiency of 98 % and 95 % respectively [12]. These efficiency ratings were typical nominal upper bounds of efficiency, resulting in the computations not underestimating the traction force while still modeling some losses.

A constant front wheel radii r was set to 0.3340m, which was a measurement obtained from previous experiments outside this project. Note that the front wheel radii was later more accurately estimated when performing the hybrid simulation computations in Section 5.

4.2.2 Normal forces

The normal forces of the car front and rear axis, as well as the trailer axis, was estimated by the force equations in Section 3.2. The car front and rear axis normal forces were also estimated by the linear relation obtained from the axle height experiment described in Section 4.1.1.

4.2.3 Pitch and slope angles

The pitch angle θ of the car could be computed at every time step by evaluating the difference in front and rear axle height. Looking at the car with its front pointing up or down relative its rear, one can see by using trigonometry that the pitch angle is

$$\theta = \arcsin \frac{Ax_F - Ax_R}{L_1}. \tag{4.1}$$

Then, by exploiting the fact that the accelerometer will have some gravity leaking into its longitudinal measurements as

$$a_{x,IMU} = \dot{v_x} + g \sin(\theta_s + \theta), \tag{4.2}$$

one can isolate the gravitational component by comparing the accelerometer measurements to differentiated wheel speeds $\dot{v_x}$. Thus, the slope angle θ_s can be found as

$$\theta_s = \arcsin\left(\frac{1}{g}(a_{x,IMU} - \dot{v_x})\right) - \theta. \tag{4.3}$$

4.2.4 Longitudinal acceleration

The longitudinal acceleration $a_{x,IMU}$ with the leaked gravity in the IMU measurements from both slope and pitch angle, was compensated for as

$$a_x = a_{x,IMU} - g \sin(\theta_s + \theta). \tag{4.4}$$

This estimate was preferred over the estimate from purely the differentiated wheel speed sensors. The reason for this was due to the inherent amplification of noise that comes with numerical differentiation of a sensor signal.

4.2.5 Longitudinal slip

The longitudinal slip was computed, assuming identical front and rear wheel radii, as

$$i = \frac{\omega_F - \omega_R}{\omega_R} \tag{4.5}$$

By using this simplified formulation of the slip, an implicit assumption is made that the front and rear wheel radii are equal. This will generally result in a nonzero offset i_{offset} in the slip to traction force F_x relationship at $F_x = 0$.

4.2.6 Car front and rear wheel radii

The car front and rear wheel radii were estimated by exploiting the fact that the wheel angular speed and the vehicle absolute speed were measured individually. First, the rear wheel radii r_R was estimated as

$$r_R = \frac{v_{GPS}}{\omega_R}. \tag{4.6}$$

For the front radii, the front wheel angular velocity needed to be compensated for the longitudinal slip offset first, so that

$$\omega_{F_{comp}} = \frac{\omega_F}{1 + i - i_{offset}}, \tag{4.7}$$

where i_{offset} is the constant offset at $F_x = 0$ in the linear relationship between F_x and i. Then, the front wheel radii could be estimated similarly to the rear wheel radii as

$$r_F = \frac{v_{GPS}}{\omega_{F_{comp}}}. \tag{4.8}$$

The front wheel radii was also estimated without the use of GPS. In this case, the rear radii was taken as its documented value r, obtained from a previous unrelated project, and the front radii was then estimated as

$$r_F = \frac{r}{1 + i - i_{offset}}. \tag{4.9}$$

4.2.7 Frequency analysis

The frequency spectrum of the system signals were computed by the FFT algorithm implemented in MATLAB. The computations were done on the signals without any prior filtering as to not loose information. The results where then smoothed after the computations for visualization purposes by a moving mean filter with a window size of 50 samples.

4.3 Parameter estimation

This section describes how parameter estimation was used to find parameters for the Force and Pitch-Bounce vehicle models.

4.3.1 Force model

This section describes a method of estimating unknown Force model parameters on collected car- and car-trailer data. By Newtons second law, the longitudinal forces described in Section 3.2 can be summed and set equal to the product of the system mass and its longitudinal acceleration, making it possible to solve for the rolling and aerodynamic resistive forces as

$$R_a + R_r = F_x - ma_x - R_{\theta_s}. \tag{4.10}$$

By computing the right hand side of (4.10) from gathered car-only sensor data, a least squares estimation can be performed of the parameters defining the car resistive forces R_{a1} and R_{r1} as

$$\begin{cases} Y_1 = R_{a1} + R_{r1} = F_x - m_1 a_x - R_{\theta_s}. \\ \phi^T = \begin{bmatrix} (v - v_{wind})^2, & \cos(\theta_s) \end{bmatrix} \\ \hat{\theta_1} = \begin{bmatrix} \frac{\rho}{2} A_{f_1} C_{d_1}, & W_1 f_{rr_1} \end{bmatrix}^T \end{cases} \tag{4.11}$$

Then, parameters for trailer resistive forces can be estimated on data with the trailer now attached. The trailer resistive forces can be separated from car resistive forces by utilizing the previously estimated car parameters $\hat{\theta_1}$ such that

$$R_1 = \phi^T \hat{\theta_1}. \tag{4.12}$$

The trailer least squares problem then become (note that this would be computed on completely different data than the previous estimation was made on)

$$\begin{cases} Y_2 = F_x - m_2 a_x - R_{\theta_s} - R_1 \\ \phi^T = \begin{bmatrix} (v - v_{wind})^2, & \cos(\theta_s) \end{bmatrix} \\ \hat{\theta_2} = \begin{bmatrix} \frac{\rho}{2} A_{f_2} C_{d_2}, & W_2 f_{rr_2} \end{bmatrix}^T \end{cases} \tag{4.13}$$

All samples with braking active, as well as the turning maneuver to be able to drive the same route back, are removed before parameter estimation. The parameter estimations in this project were performed on data gathered on the Flat driving route. For the Slope driving route, the saved parameters from the Flat driving route were simply loaded and used directly.

4.3.2 Pitch-Bounce model

The car front and rear axle stiffness parameters k_f and k_r were taken as the respective values found when performing a least squares linear fit on the relation between axle height to normal force, as shown in Figure 4.7. The stiffness parameters obtained were $k_f = 97\frac{kN}{m}$ and $k_r = 89\frac{kN}{m}$. The trailer axle stiffness was unknown. However, it was assumed to at least be larger than the car axle suspension stiffness even though the Audi had a quite stiff suspension, due to the trailer not having any dedicated suspension at all. By taking

$k_t = 3k_r$, the eigenfrequencies showed consistent results with the reference data frequencies. Assumptions also had to be made about the car and trailer inertias, I_v and I_t. For a typical passenger car, one can approximate $I_v = 3200$ [12]. For the trailer, it was assumed that its mass resisting the pitching moment was roughly distributed in such a way that it could be thought of as lumped together about half a meter away from its axis of rotation, giving $I_t = (mt + ml) \cdot 0.5^2$.

The trailer load was approximated as a point mass, as the real pallet load in the reference data was quite concentrated relative to the trailer and car. With these parameters, the characteristic equation of (3.27) could be numerically solved. By doing so, the natural frequencies of the system could be obtained as previously described in section 2.3.

Chapter 5

Hybrid simulation

In this chapter, the proposed hybrid simulation framework is described. The method tries to mimic what changes one would expect to see in collected car sensor signals if a trailer would have been attached while the car was driving.

New "hybrid" signals are computed by modifying the experimentally gathered car only sensor data with these expected trailer specific effects. Bar notation is used to distinguish between original "car-only" variables x (without bar), and hybrid variables $\bar{x}$ (with bar).

5.1 Traction force

Perhaps the first thing that one thinks of would change when attaching a trailer is that the traction force of the car would have to be greater. So the question is, how much larger should the traction force be? Since the trailer is connected to the car at the hitch, F_{hi} is the only force that is added in the longitudinal direction when attaching a trailer.

This can also be seen in the force equations in Section 3.2. By solving for F_{hi}, this force can simply be added to the original traction force F_x such that

$$\overline{F_x} = F_x + F_{hi}. \tag{5.1}$$

F_{hi} was computed from the measured trailer parameters as well as the drag and rolling resistance parameters estimated as the least squares fit to the Force model described in Section 4.3.1.

5.2 Normal forces

Hybrid car front and rear normal forces $\overline{W_F}$ and $\overline{W_R}$ were computed from the force equations in section 3.2. These equations depend on both the longitudinal and the vertical forces at the hitch F_{hi} and W_{hi}.

5.3 Axle heights

Hybrid axle heights were computed from the linear relationship found between axle height and normal forces in section 4.1.1 such that

$$\overline{Ax_F} = p_{F_1}\overline{W_F} + p_{F_2} \tag{5.2}$$

and

$$\overline{Ax_R} = p_{R_1}\overline{W_R} + p_{R_2}, \tag{5.3}$$

where F and R subscripts denote parameters related to front and rear axle, respectively.

5.4 Pitch angle

The relative change in the axle heights $\overline{\Delta Ax}$ resulting from attaching a trailer can be used to compute changes in car pitch angle θ. First, the relative change is found as

$$\overline{\Delta Ax} = (\overline{Ax_F} - Ax_F) - (\overline{Ax_R} - Ax_R). \tag{5.4}$$

The hybrid pitch angle then becomes

$$\overline{\theta} = \theta + \arcsin\frac{\overline{\Delta Ax}}{L_1}. \tag{5.5}$$

5.5 Longitudinal acceleration

If the trailer attached to the hitch of the car is not perfectly balanced at its CoG, the car pitch angle will be affected. This will lead to the measured longitudinal acceleration in the car also changing due to the amount of gravity leakage added. Thus we have that

$$\overline{a_{IMU}} = a_{x,IMU} + g\sin(\overline{\theta} - \theta) = a_{x,IMU} + g\frac{\overline{\Delta Ax}}{L_1}. \tag{5.6}$$

5.6 Car front and rear wheel radii

Hybrid car front and rear wheel radii were estimated by adding the estimated change in radii due to changes in respective car axle normal force as

$$\overline{r_R} = k_R(\overline{W_R} - W_R) + r_R, \tag{5.7}$$

and similarly for the front wheel

$$\overline{r_F} = k_F(\overline{W_F} - W_F) + r_F. \tag{5.8}$$

The tire stiffness parameters k_R and k_F where estimated from the assumed linear relationship between the slip compensated normal forces and radii estimates.

5.7 Wheel speeds and slip

For a front wheel driven car, the change in wheel speed of the rear axle can be modeled as only dependent on the normal forces, which will have modified the rear wheel radii. Since the linear velocity v of the car is supposed to be kept unchanged in the hybrid simulations, we have a constraint that

$$v = v_R = \overline{v_R}, \tag{5.9}$$

and thus

$$\omega_R r_R = \overline{\omega_R}\,\overline{r_R} \tag{5.10}$$

From here one can just rearrange and get an expression for the hybrid rear wheel angular velocity as

$$\overline{\omega_R} = \omega_R \frac{r_R}{\overline{r_R}}. \tag{5.11}$$

For the front wheels, a second effect must be taken into consideration. In addition to the wheel radii changing, the increase in traction force will increase the longitudinal slip. Since slip is a measure of how much faster the front wheel is spinning than the vehicle speed, this needs to be included in the estimate of any front wheel speeds. The constraint of equal linear velocity

$$v = v_F = \overline{v_F} \tag{5.12}$$

still holds, as the linear velocity of the front wheel should not be changed. We define the slip stiffness as

$$C_i = \frac{F_x}{i} \tag{5.13}$$

so that $C_i i = F_x$. Since C_i can be approximated as increasing linearly with the applied normal force W_F [12], we can compute the hybrid slip stiffness as

$$\overline{C_i} = C_i \frac{\overline{W_F}}{W_F}. \tag{5.14}$$

For easier notation, define the "slip slope" k_s as the reciprocal of C_i and have

$$\bar{k_s} = \frac{1}{\bar{C_i}} = k_s \frac{W_F}{\overline{W_F}}. \tag{5.15}$$

The hybrid slip is then

$$\bar{i} = \bar{k_s}\,\overline{F_x} \tag{5.16}$$

Now, we know that that the hybrid slip also has the form

$$\bar{i} = \frac{\overline{\omega_F}\,\overline{r_F} - v_F}{v_F} = \frac{\overline{\omega_F}\,\overline{r_F}}{v_F} - 1, \tag{5.17}$$

so we can rearrange and solve for $\overline{\omega_F}$ as

$$\overline{\omega_F} = \frac{v_F}{\overline{r_F}}(1 + \bar{i}). \tag{5.18}$$

The velocity v_F can also be solved for from the car-only slip equation as

$$v_F = \frac{\omega_F r_F}{1 + i}. \tag{5.19}$$

Substituting (5.19) into (5.18), the final expression for the hybrid rear wheel angular velocity becomes

$$\overline{\omega_F} = \frac{1}{\overline{r_F}} \frac{(\omega_F r_F)}{(1 + i)}(1 + \bar{i}). \tag{5.20}$$

5.8 Frequency domain and noise

Since the model used to derive the hybrid signals this far did not contain any pitch or bounce vibration dynamics, a frequency analysis would be able to tell real trailer data apart from hybrid simulated data. This did not interfere with the results for the Small trailer. For the Medium and Large trailers driving the Slope route however, it could be seen that the hybrid simulated slip to traction force had less spread in the hybrid simulated case.

The increase in mass and aerodynamic resistance, combined with less ideal driving conditions, were suspected to be the cause of the larger noise magnitude. In order to get more consistent results, normally distributed random noise was added to the hybrid wheel speed signals for the larger trailers. The noise amplitude was modeled as a sinusoidal with a frequency corresponding to the trailer frequency found in the gathered trailer data, backed up by the results obtained from the trailer Pitch-Bounce model.

5.9 Evaluation criteria

Some measures of how well the hybrid signals actually imitate the characteristics of real trailer data had to be decided. Even though the car and trailer data was gathered during similar circumstances, a direct comparison between signals over time or distance would not be a good enough measure due to unavoidable differences in driving.

A more robust approach would be comparing important variable relations against each other. By restricting the error evaluation to the traction force to longitudinal slip relationship, all important hybrid signals would still be implicitly evaluated. Since the relationship between traction force and slip can be modeled as linear, it was possible to compare linear fits of the hybrid and reference data. Specifically, the slope, offset and root mean square error (RMSE) was computed and compared. The downside of this approach was that it resulted in three error measurements, making it hard to determine total error. Due to this, a fourth standalone error measurement based on error ellipses was introduced as a complement.

First, it was assumed that the two variables of interest could be described as jointly normally distributed random variables, resulting in a bivariate distribution. This was not strictly true for some of the variables examined with this approach since they did not have a static mean. However, by allowing this simplification, error ellipses could then be computed - bounding the 2D data points at a given confidence level. This made for an intuitive and easily evaluated measure of the point clouds relation to one another. By evaluating the areas of the overlayed hybrid and reference error ellipses, and regarding all area which was not overlap as error, a relative error measure e_A was defined as

$$e_A = \frac{A_{error}}{A_{ref}}, \tag{5.21}$$

were A_{error} and A_{ref} are the error and reference areas, respectively. A 95 % confidence interval was set to capture the most relevant characteristics while discarding outliers. The confidence ellipse semi axis length was scaled by the Mahalanobis distance Δ, found by evaluating the inverse cumulative χ^2 distribution of order 2 at 95 % confidence.

To illustrate the process, Figure 5.1 show an example of how raw two dimensional data is approximated by a bivariate normal distribution, with some of the associated confidence ellipse contours drawn separately. Then, two different bivariate normal distributions are compared by their respective confidence ellipse, shown in Figure 5.2. The relationships between the estimate, reference and error ellipse areas are illustrated.

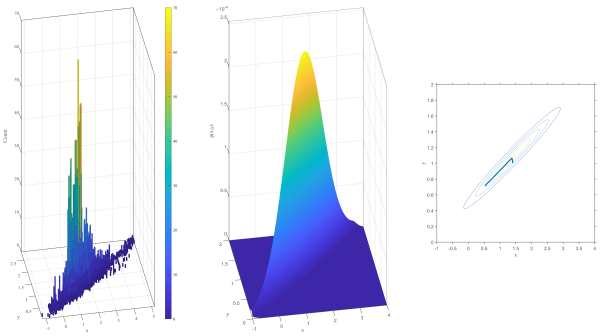

Figure 5.1 – Example showing bivariate data (traction force versus slip). In the first plot a 2D histogram of the raw sensor signals is shown. In the second plot the data is approximated as a bivariate normal distribution. In the third plot, isoprobability (equal density) contours are shown taking the shape of ellipses.

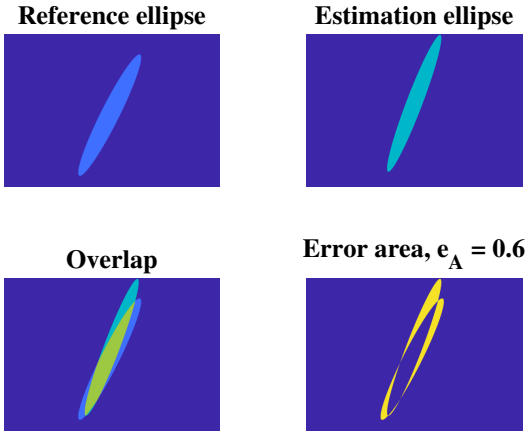

Figure 5.2 – Example of the ellipse error area measure e_A, relating the error area to the reference area.

Chapter 6

Results

In this chapter, the main results are shown. The Force model is compared to the gathered data in Section 6.1, both with nominal and fitted parameters. The results of the suggested hybrid simulation method of artificially attaching a trailer to car data, built upon the results of previous chapters, are shown in Section 6.2.

Finally, the vibration frequencies of the car-trailer system, found both in the collected data and estimated by the Pitch-Bounce model, are shown in Section 6.3.

6.1 Force model

The estimated parameters for the force model are shown in Table 6.1. The estimates of the car parameters are close to the expected values. The estimated trailer parameters are within reasonable bounds of what could be expected.

The trailer parameters in the "Expected" column include a large amount of uncertainty, since they are extrapolated from cars, vans and buses, and should therefore not be taken to be ground truth. The aerodynamic drag coefficient increases with trailer size, which was expected due to the shapes of the trailers. The rolling resistance coefficients were slightly higher for the trailers than the car.

Table 6.1 – Estimated model parameters. Expected parameters in parenthesis indicate that it is an assumption with greater uncertainty than that of an expected value from a datasheet or empirical studies.

Parameter estimation		
Parameter	**Estimate**	**Expected**
C_d car [−]	0.32	0.28
C_d Small trailer [−]	0.47	(0.4)
C_d Medium trailer [−]	0.57	(0.6)
C_d Large trailer [−]	0.70	(0.8)
f_{rr} car [−]	0.0132	0.013
f_{rr} Small trailer [−]	0.0197	0.013
f_{rr} Medium trailer [−]	0.0166	0.013
f_{rr} Large trailer [−]	0.0153	0.013

Residuals from the Force model least squares parameter estimation are shown in Figure

6.1. A large vertical offset in the residuals, occurring after turning to drive the same way back at 5000m, is clearly seen in the left plot. The offset is largely removed when compensating for the wind, as shown in the right plot. No other residual dependency could be seen when plotting residuals against other variables such as velocity or accelerations.

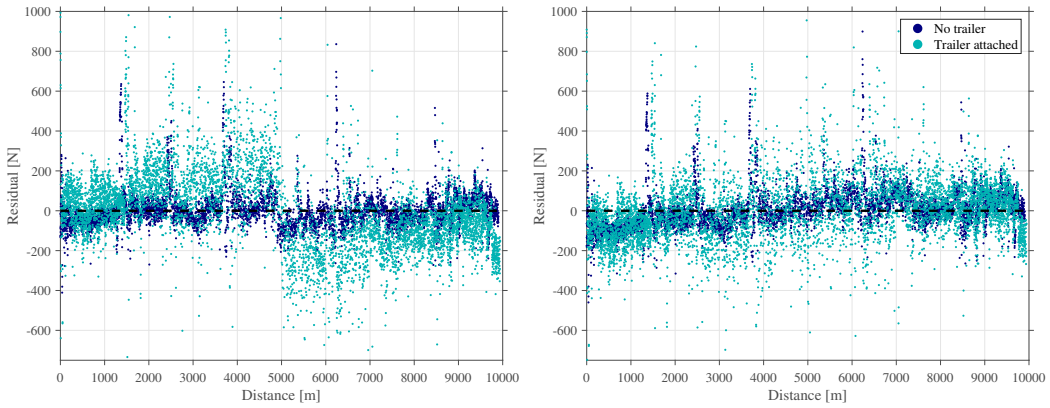

(a) No wind compensation. **(b)** Wind compensation activated.

Figure 6.1 – Residuals from the least squares parameter estimation, plotted over distance. At 5000m, the car turns to drive the same road back. The residuals show a significant dependence on the wind direction. When compensating for wind, the residual offset is almost completely removed.

The coefficient of determination (R-squared) for the Force model least squares fit as well as the nominal parameters are shown in Table 6.2. A coefficient of 1 means that the model output completely explains the variance in the data. It is clear that a slightly lesser amount of variability in the response variable is explained by the model when attaching a trailer. This is in part due to the error propagation stemming from using the car only estimates to do further estimation of trailer parameters. As expected, the least squares fit gives a better (higher) coefficient of determination than the nominal parameters, but only slightly higher.

Table 6.2 – Comparing coefficient of determination (R-squared) of the Force model with parameters from least squares fit and nominal values.

Coefficient of determination (R-squared)			
Route	**Driving case**	**LS fit**	**Nom. params**
Flat	Car only	0.940	0.939
Flat	Small trailer	0.774	0.730
Flat	Medium trailer	0.862	0.861
Flat	Large trailer	0.842	0.824
Slope	Car only	0.950	0.931
Slope	Small trailer	0.890	0.811
Slope	Medium trailer	0.884	0.883
Slope	Large trailer	0.909	0.905

6.2 Hybrid simulation

In this section, the hybrid simulation results are presented. Longitudinal slip and traction force will be used to illustrate the results since they depend on all the important computed hybrid signals. A simple case of slip and traction force hybrid simulation results are shown plotted against each other in Figure 6.2. The difference between the car-only and trailer reference data is captured by the artificially attached trailer (hybrid simulation).

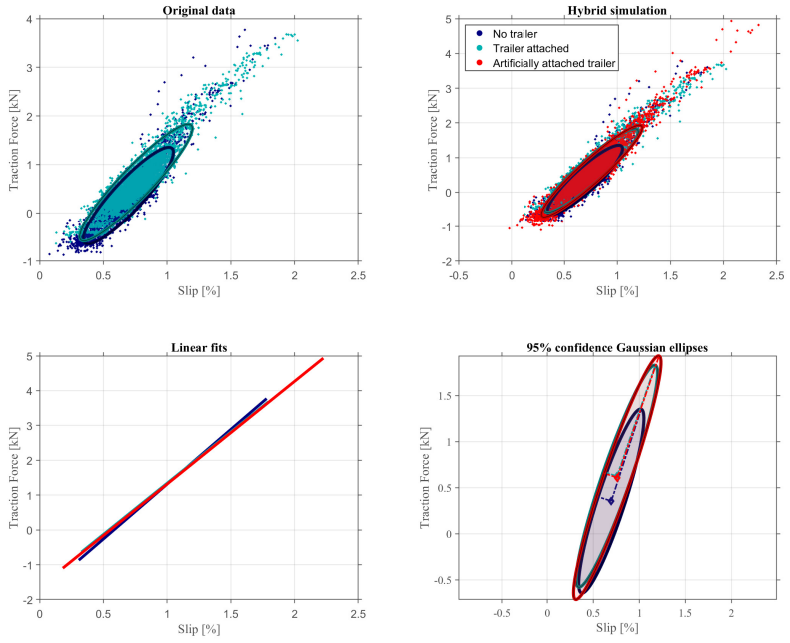

Figure 6.2 – Hybrid simulation. The artificially attached trailer data closely match the reference trailer data points and its corresponding 95 % confidence ellipse and linear fit.

When moving the trailer load to front and rear positions, both offsets and changes in the slip slope of the trailer point clouds occurs, seen in Figure 6.3. The hybrid simulation model captures these effects as well, seen by the overlap of point clouds and confidence ellipses. Further illustrations by box plots and kernel density estimates of how the hybrid simulated slip handles longitudinal trailer load transfer are shown in Figure 6.4.

Hybrid simulation results of the Large trailer in the Slope route are shown in Figure 6.5, highlighting still good performance on the least ideal driving route in combination with having the heaviest and largest trailer attached. However, for the Medium and Large trailer specifically in the Slope driving route, some noise had to be added to the wheel speed signals in order to get the same amount of spread in slip as the reference data. It can be seen that the data points and confidence ellipses of the trailer reference and hybrid simulated data show more consistency in Figure 6.5b than in Figure 6.5a.

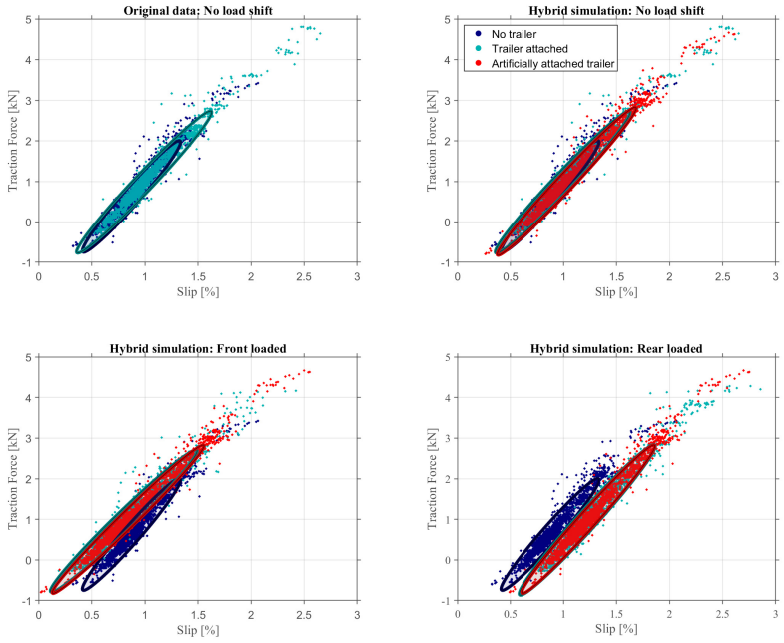

Figure 6.3 – Hybrid simulation, all load cases, Slope route. The artificially attached trailer data follow the offset and slope shifts of the reference trailer data points and its corresponding 95 % confidence ellipse.

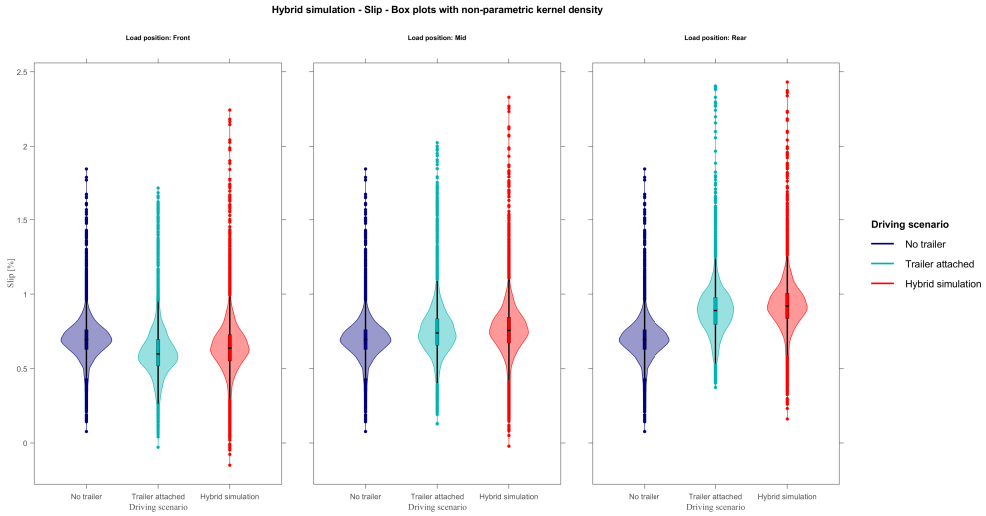

Figure 6.4 – Box plots and kernel density estimates of reference car and trailer data, as well as the hybrid simulated trailer data. Flat route. The plot shows the hybrid simulated trailer following the reference trailer data by having its median offset and its density shape compressed.

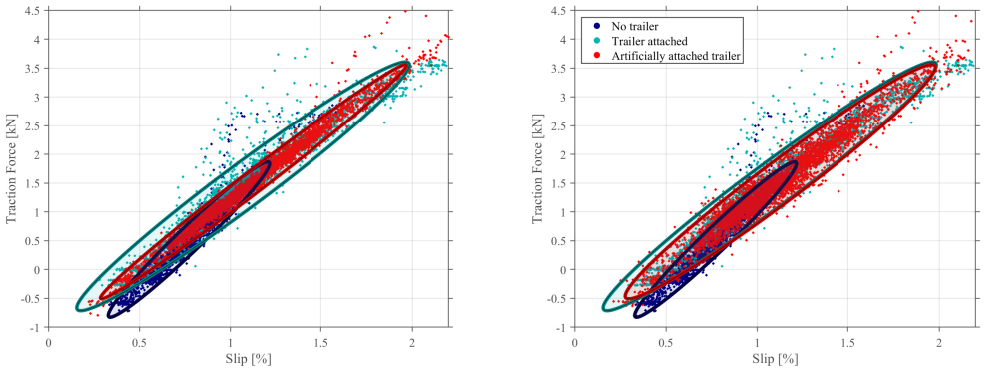

(a) No noise added. **(b)** Noise added.

Figure 6.5 – Hybrid simulation. Large trailer, Slope driving route. The top plot shows the hybrid simulation matching the change in offset, slope and major axis spread, but not the minor axis spread in the trailer data points. The bottom plot shows the same hybrid simulated signals but with the addition of noise to the wheel speed signals.

The error measures described in Chapter 5 determining similarity between hybrid simulation to reference trailer data, are shown in Table 6.3. Overall, a low error is obtained for all scenarios.

Table 6.3 – Hybrid simulation slip error, sorted from largest to lowest area error e_A.

Hybrid simulation slip error						
Route	**Trailer**	**LoadPos**	**Slope diff**	**Offset diff**	**STD diff**	e_A
Slope	Small	Mid	-0.0023	0.0327	-0.0046	0.340
Slope	Small	Front	-0.0010	0.0255	-0.0065	0.264
Flat	Small	Rear	-0.0014	0.0288	-0.0028	0.242
Slope	Medium	-	-0.0042	0.0025	0.0110	0.178
Slope	Large	-	-0.0049	0.0317	-0.0070	0.178
Flat	Large	-	-0.0018	0.0227	-0.0117	0.175
Flat	Small	Front	-0.0008	0.0177	-0.0017	0.160
Flat	Medium	-	0.0034	0.0107	-0.0104	0.147
Slope	Small	Rear	-0.0015	0.0059	-0.0058	0.141
Flat	Small	Mid	-0.0012	0.0103	-0.0032	0.125

6.3 Pitch-Bounce model

The frequency spectrum of the longitudinal acceleration a_x and pitch angle θ are shown in Figure 6.6a. The top plot highlights the load positional dependent 3 Hz peak that attaching the Small trailer resulted in. No such peak could be seen in the car-only signals, which confirms that this is a trailer specific effect.

The bottom plot shows energy in the frequency ranges of 1-2.5 Hz. This corresponds to the expected pitch and bounce frequencies for most passenger cars, where the bounce natural frequency usually is between 1.0 - 1.5 Hz and the pitch natural frequency "slightly higher than that for bounce" [12]. No clear trailer or trailer load dependency can be seen for these frequencies. These results agree with the Pitch-Bounce model estimates.

No 3 Hz peaks appear in the computed pitch angle θ however, which is estimated from low resolution axle height sensors.

The frequency spectrum of the front and rear axle heights are shown in Figure 6.6b. The pitch angle θ is computed from these two sensor signals, so similar behavior is expected. However, it is now clear that the large peak in θ in Figure 6.6a comes from the rear axle (rear loaded case).

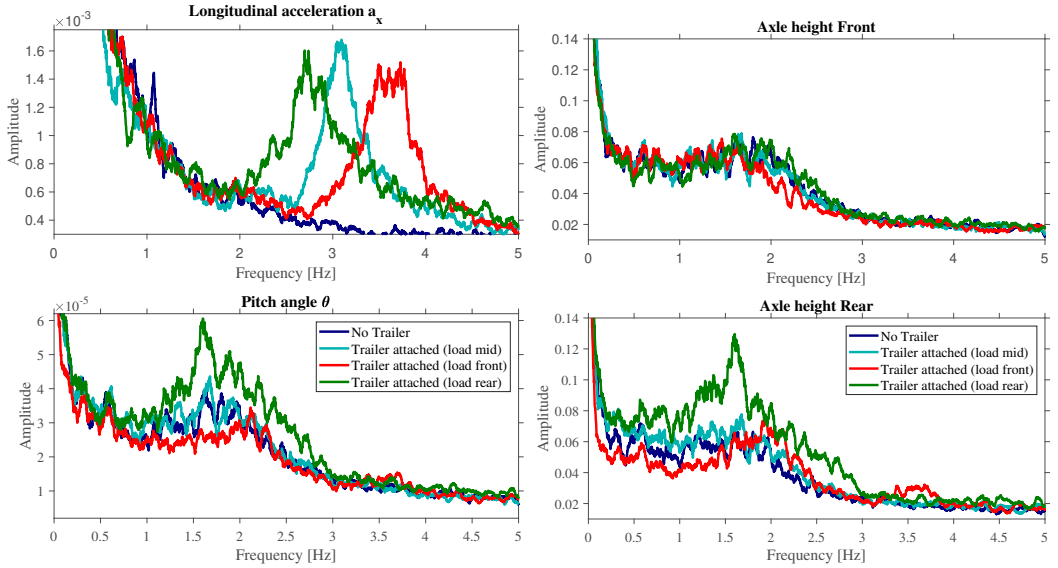

(a) The prominent 3 Hz peak in a_x does not appear unless a trailer is connected. The peak shifts to higher frequencies the closer the trailer load is moved towards the towing car.

(b) Most energy is present in the frequency ranges of 1-2 Hz. No clear trailer or load frequency dependency can be seen, except from the large peak in the rear axle plot for the rear loaded trailer.

Figure 6.6 – Frequency analysis of the Small trailer, varying trailer load positions.

Figure 6.7 shows the frequency spectrum of the same variables as in Figure 6.6a but for all three trailer types.

The natural frequencies of the Pitch-Bounce model are shown in Table 6.4 for the different load cases of the Small trailer. The observed frequency peaks of a_x and θ in the frequency spectrum are included as reference. The first two model frequencies, ω_{n_1} and ω_{n_2}, stay stationary as the trailer load is moved from rear to front, while ω_{n_3} vary with the load being moved inside the trailer. In the reference data, the load dependency is clearly seen in how

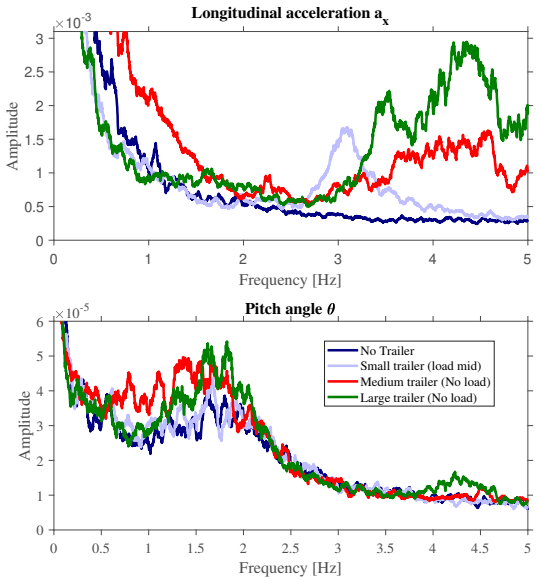

Figure 6.7 – The model estimate eigenfrequencies only in the lower half of the spectrum for the Medium and Large trailer. However, the sensor data show energy not only at these frequencies but also at higher frequencies than for the Small trailer. The Large trailer have a pronounced peak at 4.2 Hz in the pitch angle plot. The Medium trailer has a plateau between 3.7 and 4.7 Hz.

a_x increases with the load being moved closed to the car. The frequency peaks are more stationary in θ, and does not depend on having a trailer connected or not. Since both these characteristics are captured, it can be concluded that the model frequencies show qualitative consistency with the reference data frequencies.

Table 6.4 – Natural frequencies of the Pitch-Bounce model for the different load cases of the Small trailer. The observed frequency peaks of a_x and θ in the gathered data are included as reference.

System natural frequencies [Hz]					
Trailer	ω_{n_1}	ω_{n_2}	ω_{n_3}	**FFT**(a_x)	**FFT**(θ)
No trailer	1.51	1.67	-	-	1.6
Small (rear)	1.50	1.58	2.81	2.7	1.6
Small (mid)	1.51	1.61	3.04	3.1	1.7
Small (front)	1.50	1.57	3.54	3.6	2.1
Medium (empty)	1.50	1.58	1.93	(4.1)	(1.4)
Large (empty)	1.27	1.49	1.55	(4.3)	(1.6)

Chapter 7

Discussion

The purpose of the thesis, to investigate and model what physical phenomena are associated with having a trailer connected to a car, relevant for TPI, was achieved. The derived car-trailer model showed similar results to the gathered sensor data. The goal of this thesis, constructing a hybrid simulation framework making it possible to artificially attach a trailer to collected car data without trailer, was also achieved.

By evaluating the Gantt scheme every week, the work was adjusted as to not fall behind in the planning. One such adjustment was regarding the initial intent to rank the impact of the physical phenomena of trailers on TPI in relation to each other by a sensitivity analysis. This was ultimately not done due to lack of time and prioritizing other topics deemed more important for the thesis, such as the hybrid simulations.

7.1 Data gathering and vehicle dynamics computations

The two driving routes used in this project met almost all desired criteria, most likely as good as one could hope for apart from a race or testing track. The Slope route was not as straight as the Flat route, resulting in some lateral force and acceleration disturbances, but these were of small magnitude and should not influence the results.

The main thing that could have been done to reduce disturbances would have been postponing the experimental data gathering on days with higher wind speeds than the standards SAE J1263 and FCA 7-T3040 suggest [26]. The wind speeds were higher on all four days of data gathering than FCA 7-T3040 and higher on three of the four days than SAE J1263 suggest. To set the wind speed to perspective, the wind speed was about half the car mean speed. As the drag force is proportional to the square of the car relative wind speed, even small errors have significance. The effect is clearly seen in Figure 6.1.

While the added wind compensation greatly improved the results to the point of the residuals barely showing any directional dependence, it certainly would have been better without it. This became clear when estimating model parameters on data that was gathered on the windiest days, as the estimations were quite sensitive to how the wind compensation was tuned. An alternative to postponing the data collection sessions could have been to mount an anemometer on the car, which would measure the wind speed relative the car. This would at least give a better input to the drag force computations than treating the wind as a constant.

The wind could also have been modeled as varying instead of just a constant since the approximate wind bearing was known. Depending on the heading of the car at each given

time step, the wind magnitude would then be scaled accordingly.

For the Flat route tests however, where car and trailer parameters were estimated, the heading of the car did not vary that much in each direction. A larger improvement might have been noticed on the Slope route tests due to the larger route curvature. Due to the residuals of the least squares estimates behaving similarly for each route though, this implementation was not prioritized but should be possible to do in any future work.

7.2 Force model

The force model captured the physics of the car to the extent of closely recovering the car datasheet drag coefficient as well as the standard rolling resistance coefficient on asphalt. It also proved to be of high enough fidelity to use in the hybrid simulations, mimicking the effects attaching a trailer would have on the car sensor signals.

The procedure of first estimating car parameters and then using these estimates on other data for further estimation of trailer parameters introduces error propagation. However, without sensors mounted on the trailer, this was deemed the only feasible way of separating the measured forces and parameters.

Take the added longitudinal force at the hitch, F_{hi}, as an example. The expression for computing F_{hi} is not complicated but it requires some trailer specific parameters. The dimensions were easy to measure, and the weight and CoG was possible to measure in the garage experiments described in Section 4.1.1. The drag coefficient however is very complex, depending on what assumptions and simplifications are made. The total drag force of a given car-trailer system can not be obtained by estimating drag for the vehicles separately in for example a wind tunnel and then simply adding them back together. The reason for this is that the combination of car and the trailer geometry will affect how the air will flow [12]. In this project however, where a specific car and car-trailer combinations where used for the driving tests, it was the total increase in drag due to attaching different trailers that was estimated. This means that the additional drag caused by adding a trailer included changing the character of air flow for both car and trailer.

An example of this is turbulence in the gap between the car and trailer. For passenger cars with similar geometry to the Audi A6 Avant though, the difference could be assumed negligible. With higher speeds the difference would become larger, but the max speed of 80 km/h puts a bound on how fast one should need to worry about. And while these errors would be troublesome if one wanted to estimate the additionally required force for a specific car-trailer combination, that was not the end goal of this project. Instead, what was important was the qualitative changes of attaching trailers of varying sizes, not replicating exact car-trailer combinations. So, while it was also important that all phenomenon of the car-trailer data gathered were explainable with the models used here, the ultimate goal was to have a model that generalized the qualitative changes of having trailers of different types attached to a passenger car.

More complexity could be added by modeling for example aerodynamic lift, which might have a larger impact on the trailers than on the car. The reason for why this might be is that the characteristic lift area of would be larger for trailers of medium to large sizes than that of the car, while at the same time in many cases having lower normal forces, opposing the lifting force, than the car.

Adding complexity like this would however come at the cost of needing to estimate another parameter, in this case the product of the vehicle lift area and the aerodynamic lift

coefficient. For the purposes of this project, the added complexity was not deemed worth the cost of potentially risking worse estimates for the major force contributors.

For future work, more advanced driving routes with sharper turns and thus larger lateral forces would benefit from having the lateral dynamics included in the model. A model for the brakes could also be included, instead of removing the braking segments as was done here.

Modeling the braking dynamics would however probably require a nonlinear ODE model to be solved by iteration, increasing both complexity and sensitivity significantly to initial values. This was actually attempted during the project but later abandoned due to the output never reaching the same levels of generalized accuracy that the simpler Force model achieved. As TPI is inactive during braking, the reasoning was that modeling braking would not add significant value for the end goal of evaluating TPI performance.

7.3 Hybrid simulation

The hybrid simulations showed good consistency for all three trailers with low error measures in offset, slope, variance and ellipse error area. As a next step, it would be interesting to test the method on more data to see how well it generalizes. There are also improvements that could be made both in the point cloud error measure e_a as well as investigating how to model the noise more rigorous.

Instead of assuming normal distribution of the sensor signals and thus elliptic probability densities, one could perhaps use bivariate non-parametric distributions, similar to the univariate ones shown in Figure 6.4, instead. An approach like this would better capture the spread of the gathered data, and could make point cloud area comparisons more accurate. This could potentially require a larger amount of data to be collected for each signal to get a good distribution estimate though, as one would disregard any knowledge about the expected point cloud shape, making the approach more sensitive to outliers.

The additive noise that was added to the wheel speed signals to emulate noise induced by the Medium and Large trailer could be modeled less ad hoc than just adding sinusoidal Gaussian noise with constant amplitude. The flaws of this approach can be seen in the Figure 6.5, where the added noise has successfully broadened the point distribution in the minor semi axis direction but at the cost of outliers appearing further up the major axis direction than the trailer reference data points.

One could imagine that the noise amplitude would depend on many variables such as trailer size, weight, loading, suspension, as well as system longitudinal acceleration, traction force, velocity and road surface evenness. Such an investigation was outside the scope of this thesis but is something that future work could investigate further.

7.4 Pitch-Bounce model

The Pitch-Bounce model showed good consistency with the frequencies observed for the Small trailer. Both the assumed bounce and pitch frequency of the car between 1-2 Hz seems to have been captured, as well as the trailer frequency at 3 Hz. The load positional dependency of the trailer frequency was captured as well.

It is not completely clear why these frequencies could only be observed in a_x and not in θ. It might be due to the IMU, where a_x is computed from, being more sensitive to

low amplitude vibrations than the axle height sensors, where θ is computed from. The axle height sensors had a resolution of only 2mm, which means that low amplitude oscillations might pass unnoticed. Regarding the rear loaded trailer specifically, it exhibited a significantly larger resonance peak in θ than the other load cases. A rear loaded trailer decreases stability, which could possibly be what increased the vibration amplitudes in the car.

The frequency content of the Medium and Large trailers were located in the higher part of the spectrum and was not predicted by the model. In the longitudinal acceleration, the high and prominent peaks of the Medium and Large trailers might come from something more related to longitudinal motion. However, given that at least the Large trailer have coinciding peaks at 4.2 Hz in both a_x and θ, it is hard to disregard the possibility that it represents something that the model might missed to capture.

It is important to note though that the model was designed for a trailer with only one axle, while the Medium trailer had two and the Large trailer had three. These two trailers also had mechanical braking systems and some kind of suspension, which was not taken into consideration. The lower frequency content of these trailers showed consistency with the model though, making them still interesting to evaluate.

This thesis was focused on the relative wheel radii estimation part of TPI and not the vibration analysis part. As such, the results from this frequency model does not directly affect the results of the proposed hybrid simulation framework at this stage.

For future development, especially for the frequency monitoring part of TPI, these results could be interesting to investigate further though. Other application could also be possible, for example estimating the load position of an attached trailer based on peak locations in the longitudinal acceleration frequency spectrum.

7.5 Economic, social, and ecological effects

Having underinflated tires increases tire wear, fuel consumption as well as reducing vehicle handling capability. Tire Pressure Monitoring Systems are due to this both important in both economic, ecologic and safety aspects. With an indirect Tire Pressure Monitoring System such as TPI, there is no additional environmental impact as opposed to having dedicated pressure sensors mounted on each tire.

The proposed hybrid simulation framework could be easily automated and used by any engineer working on evaluating the effects of artificially attaching a trailer to car sensor data. The computations are fast and would not require the use of real vehicles, making it cost effective in regards to both time spent but also material costs. Due to the method not requiring gathering data with a real car-trailer system, it has great potential to also reduce CO_2 emissions.

Chapter 8

Conclusions

The physical phenomena associated with having a trailer connected to a car, relevant for TPI, were investigated by data gathering, modeling and simulations. The Force model captured the physics of the car to the extent of closely recovering the expected drag and rolling resistance coefficients. Further, the model was able to capture the main effects of attaching a trailer, showing still high R-squared values for the collected trailer data.

A hybrid simulation framework was proposed, where car sensor signals are modified to mimic having different types of trailers attached. The hybrid simulation results show close resemblance to the gathered data where actual trailers were connected.

By not requiring real trailer data to evaluate software performance on, the proposed framework opens up the possibility to simulate data from a much larger number of trailer combinations than would otherwise have been feasible to test in real vehicle tests. Additionally, it has great potential to lower both test related costs and CO_2 emissions.

8.1 Limitations

No lateral dynamics were modeled, making the possible driving scenarios somewhat limited to not include high lateral accelerations or routes with rapidly changing curvature.

Since all data samples containing braking were removed, aggressive braking could introduce dynamics that would be appear even after the braking removal and be of a significant enough size that the model accuracy itself would be significantly affected.

8.2 Future work

The hybrid simulation method showed great promise on the data used in this project, but should be evaluated on a larger sample size in any future work to ensure that it generalizes well. Further, lateral dynamics could be included to cover a wider variety of driving scenarios, including high curvature routes and rapid steering movements.

A more sophisticated trailer noise model could also be added, where the noise would depend both on trailer specific parameters as well as available sensor signals.

The frequency peak appearing when attaching a trailer and its trailer load dependency could be interesting to investigate further. It could serve as a starting point for working with hybrid simulations directed at the vibration monitoring part of TPI. Other use cases could also be possible, for example estimating the load position of an attached trailer based

on peak locations in the longitudinal acceleration frequency spectrum. Knowledge of the trailer load position could potentially improve load compensation algorithms.

References

[1] National Highway Traffic Safety Administration, "Federal Motor Vehicle Safety Standard (FMVSS) 138," 2005.

[2] United Nations, "UN Regulation No. 141 - Tyre Pressure Monitoring Systems (TPMS)," 2014.

[3] NIRA Dynamics, "Tire Pressure Indicator by NIRA." https://niradynamics.se/tire-pressure-indicator/ (retrieved 2021-05-25).

[4] L. Plöchl, "Improvements of passenger car-trailer behaviour by a trailer based control system," *Vehicle system dynamics*, vol. 29, p. 438–450, 1998.

[5] K. Kayacan, "Nonlinear modeling and identification of an autonomous tractor–trailer system," *Computers and electronics in agriculture*, vol. 106, p. 1–10, 2014.

[6] S. Kushairi, "Tractor-trailer modelling and validation," *International journal of heavy vehicle systems*, vol. 21, p. 64–82, 2014.

[7] T. Zanchetta, "Trailer control through vehicle yaw moment control: Theoretical analysis and experimental assessment," *Mechatronics*, vol. 64, p. 102282, 2019.

[8] P. Nilsson and K. Tagesson, "Single-track models of an A-double heavy vehicle combination," tech. rep., Department of Applied Mechanicsems, Chalmers university of technology, Göteborg, Sweden, 2013.

[9] J. Ellis, *Vehicle Dynamics*. London: Business Books Limited, 1969.

[10] R. Anderson and E. Kurtz, "Handling-characteristics simulations of car-trailer systems," tech. rep., Society of Automotive Engineers, 1980.

[11] MSC Software, "Adams car." https://www.mscsoftware.com/product/adams-car (retrieved 2021-01-28).

[12] J. Wong, *Theory of Ground Vehicles*. Wiley, 2008.

[13] R. He, "A comparative study of car-trailer dynamics models," *SAE International journal of passenger cars. Mechanical systems*, vol. 6, pp. 177–186, 2013.

[14] Institute of Electrical and Electronics Engineers (IEEE), "IEEE Code of Ethics," June 2020.

[15] B. I. et.al., "A code of ethics for robotics engineers," *ACM/IEEE Int. Conf. Human-Robot Interaction*, pp. 103– 104, March 2010.

[16] G. Veruggio and F. Operto, *Roboethics: Social and Ethical Implications of Robotics*, pp. 1499–1524. January 2008.

[17] C. M. Bishop, *Pattern Recognition and Machine Learning*. Cambridge: Springer, 2006.

[18] P. C. Mahalanobis, "On the generalised distance in statistics," *Proceedings of the National Institute of Sciences of India*, vol. 2, no. 1, pp. 49–55, 1936.

[19] B. Wang, W. Shi, and Z. Miao, "Confidence analysis of standard deviational ellipse and its extension into higher dimensional euclidean space," *PLOS ONE*, vol. 10, pp. 1–17, March 2015.

[20] K. Åström and Wittenmark, *Adaptive control*. Mineola, N.Y: Dover ed., 2008.

[21] T. Gillespie, *Fundamentals of Vehicle Dynamics*. Premiere Series Bks, Society of Automotive Engineers, 1992.

[22] H. Bauer, *Automotive handbook*. Stuttgart: Robert Bosch, 2000.

[23] H. Pacejka, *Tire and Vehicle Dynamics*. Butterworth-Heinemann, 2012.

[24] Weather database, "RL." https://rl.se/vadret/historik.php (retrieved 2021-04-05).

[25] A. Altinisik, "Aerodynamic coastdown analysis of a passenger car for various configurations," *International Journal of Automotive Technology*, vol. 18, no. 2, pp. 245–254, 2017.

[26] I. Preda, D. Covaciu, and G. Ciolan, "Coast down test – theoretical and experimental approach," October 2010.

[27] Technical Committee : ISO/TC 31/SC 3 Passenger car tyres and rims, "Passenger car tyres — Methods of measuring rolling resistance," *ICS : 83.160.10 Road vehicle tyres*, 1992.